

**CERIUM PROMOTED Ni/MGO CATALYST FOR
GLYCEROL REFORMING**

TAN WEI JIAN

**BACHELOR OF CHEMICAL ENGINEERING UNIVERSITI MALAYSIA
PAHANG**

©TAN WEI JIAN

Thesis Access Form

No _____ Location _____

Author :

Title :

Status of access OPEN / RESTRICTED / CONFIDENTIAL

Moratorium period: _____ years, ending _____ / _____ 200_____

Conditions of access proved by (CAPITALS): DR CHENG CHIN KUI

Supervisor (Signature).....

Faculty:

Author's Declaration: *I agree the following conditions:*

OPEN access work shall be made available (in the University and externally) and reproduced as necessary at the discretion of the University Librarian or Head of Department. It may also be copied by the British Library in microfilm or other form for supply to requesting libraries or individuals, subject to an indication of intended use for non-publishing purposes in the following form, placed on the copy and on any covering document or label.

The statement itself shall apply to ALL copies:

This copy has been supplied on the understanding that it is copyright material and that no quotation from the thesis may be published without proper acknowledgement.

Restricted/confidential work: All access and any photocopying shall be strictly subject to written permission from the University Head of Department and any external sponsor, if any.

Author's signature.....**Date:**

users declaration: for signature during any Moratorium period (Not Open work):

I undertake to uphold the above conditions:

Date	Name (CAPITALS)	Signature	Address

CERIUM PROMOTED NI/MGO CATALYST FOR GLYCEROL REFORMING

TAN WEI JIAN

Thesis submitted in partial fulfillment of the requirements
for the award of the degree of
Bachelor of Chemical Engineering

**Faculty of Chemical & Natural Resources Engineering
UNIVERSITI MALAYSIA PAHANG**

MAY 2014

© TAN WEI JIAN (2014)

SUPERVISOR'S DECLARATION

We hereby declare that we have checked this thesis and in my opinion, this thesis is adequate in terms of scope and quality for the award of the degree of Bachelor of Chemical Engineering.

Signature :

Name of main supervisor : DR. CHENG CHIN KUI

Position : SENIOR LECTURER

Date : 4th JUNE 2014

STUDENT'S DECLARATION

I declare that this thesis entitled 'Cerium-promoted Ni/MgO Catalyst for Glycerol Reforming' is the result of my own research except as cited in references. The thesis has not been accepted for any degree and is not concurrently submitted in candidature of any other degree.

Signature :
Name : TAN WEI JIAN
ID No : KA10072
Date : FEBRUARY 2014

Dedication

Special Dedication of This Appreciative Feeling to My...

Family, Lecturer and Friends

For Their Assistance, Encouragement and Wishes

ACKNOWLEDGEMENT

I wish to convey my hearty appreciation to my supervisor, Dr. Cheng Chin Kui for his opinion, advices, motivation, friendship, endless support, guidance and encouragement throughout the Undergraduate Research Project. I also feel thankful to my family and friends for their assistance and motivation in the thesis progress. Without their help, I may not be able to complete my thesis. I am also impassioned to University Malaysia Pahang (UMP) for supplying the facilities for my research.

Finally, I am beholden to everybody that assisted me directly or indirectly in completing this thesis.

ABSTARCT

Hydrogen (H₂) has been considered as energy of future to substitute fossil fuel utilization. It is currently produced from hydrocarbon reforming (i.e. natural gas and petroleum) and electrolysis processes. Therefore, in the current work, magnesium oxide (MgO)-supported Ni catalyst with Cerium, Ce as a promoter was prepared to produce the synthesis gas H₂ from the glycerol reforming reaction and the activity of catalyst is studied. Besides, the physicochemical properties of fresh catalysts were characterized with various techniques. BET characterization of both fresh 3 wt% and 5 wt% Ce-Ni/MgO catalysts showed that the 5 wt% Ce-Ni/MgO catalyst has larger BET specific surface area and pore diameter than the 3 wt% Ce-Ni/MgO catalyst. XRD diffraction pattern of fresh 5 wt% Ce-Ni/MgO catalyst showed peaks representing MgO at $2\theta = 37.00^\circ$ and NiO at 42.99° , 62.41° , 74.84° and 78.79° . From the FESEM imaging of 5 wt% Ce-Ni/MgO catalyst, it can be observed that it is a crystalline catalyst. TGA results summarized that the magnitude of the highest peak increases as the heating ramp increases from 10 to 20 °C/min. Besides that, reaction studies have found that the 3 wt% catalysts gave almost equal rate of formation of product yield (H₂ and CO). From the results obtained, the glycerol conversion, X_G was directly proportional with the reactant (glycerol to N₂) flow ratios. Furthermore, the activation energy obtained for H₂ formation rate from the current study was 27.82 kJ/mol. The fairly low E_a indicated that the catalyst was very active in promoting the hydrogen production from the glycerol.

ABSTRAK

Hidrogen (H_2) telah dianggap sebagai tenaga alternative pada masa depan untuk menggantikan penggunaan bahan api fosil. Ia dihasilkan daripada hidrokarbon pembaharuan (iaitu gas asli dan petroleum) dan elektrolisis proses. Oleh itu, dalam kajian ini, magnesium oksida (MgO) disokong Ni pemangkin dengan Serium, Ce sebagai penganjur yang telah disediakan untuk menghasilkan gas H_2 sintesis dari gliserol pembaharuan dan aktiviti pemangkin juga ditelitikan. Selain itu, sifat-sifat fizikokimia pemangkin telah dicirikan dengan pelbagai teknik. BET pencirian bagi 3 wt% dan 5 wt% pemangkin segar Ce-Ni/MgO menunjukkan bahawa 5 wt% Ce-Ni/MgO pemangkin mengandungi kawasan permukaan spesifik dan diameter liang yang lebih besar daripada 3 wt% Ce-Ni/MgO. Selain itu, corak pembelauan XRD bagi 5 wt% Ce-Ni/MgO pemangkin pula menunjukkan puncak yang mewakili MgO di $2\theta = 37.00^\circ$ dan NiO pada 42.99° , 62.41° , 74.84° dan 78.79° . Dari keputusan pengimejan FESEM 5 wt% Ce-Ni/MgO, dapat diperhatikan bahawa ia merupakan pemangkin kristal. Keputusan TGA juga merumuskan bahawa magnitud puncak tertinggi meningkat apabila tanjakan pemanasan bertambah dari 10 hingga 20 $^\circ C/min$. Selain itu, kajian reaksi telah mendapati bahawa 3 wt% pemangkin memberikan kadar pembentukan hasil produk (H_2 dan CO) yang hampir sama. Sehubungan itu, keputusan tindak balas juga memaparkan bahawa purata penukaran gliserol, XG adalah sejajar dengan nisbah aliran bahan tindak balas (gliserol : N_2). Tambahan pula, tenaga pengaktifan, E_a yang diperolehi bagi kadar pembentukan H_2 daripada kajian ini adalah 27.82 kJ/mol. Tenaga pengaktifan yang agak rendah tersebut menunjukkan bahawa pemangkin sangat aktif dalam menggalakkan pembentukan gas H_2 daripada gliserol.

TABLE OF CONTENTS

SUPERVISOR’S DECLARATION.....	iv
STUDENT’S DECLARATION.....	v
<i>Dedication</i>	vi
ACKNOWLEDGEMENT.....	vii
ABSTRACT.....	viii
ABSTRAK.....	ix
TABLE OF CONTENTS.....	x
LIST OF FIGURES.....	xii
LIST OF TABLES.....	xiv
LIST OF ABBREVIATIONS.....	xv
LIST OF ABBREVIATIONS.....	xvi
1 INTRODUCTION.....	1
1.1 Background.....	1
1.2 Problem Statement.....	3
1.3 Objective.....	4
1.4 Scope of study.....	4
2 LITERATURE REVIEW.....	5
2.1 Introduction.....	5
2.2 Steam Reforming Reaction of Glycerol.....	6
2.3 Dry Reforming Reaction of Glycerol.....	7
2.4 Partial Oxidation Reforming.....	8
2.5 Auto-thermal Reforming.....	9
2.6 Thermodynamics Analysis of Reactions in Glycerol Dry Reforming.....	10
2.6.1 Carbon Dioxide Conversion.....	11
2.6.2 Hydrogen and Synthesis Gas Production.....	12
2.7 Catalyst Used For Reforming Reaction.....	15
2.8 Catalyst preparation methods for reforming reaction.....	19
2.9 Catalyst Deactivation.....	19
2.9.1 Carbon Deposition.....	21
2.9.2 Poisoning.....	22
2.9.3 Catalyst Sintering.....	23
3 METHODOLOGY.....	25
3.1 Introduction.....	25
3.2 Materials.....	25
3.2.1 Chemicals for catalyst synthesis.....	25
3.2.2 Gases.....	26
3.2.3 Glycerol.....	26
3.3 Catalyst Preparation.....	27
3.4 Catalyst Characterization.....	27
3.4.1 X-ray diffraction (XRD).....	28
3.4.2 Brunauer Emmett-Teller (BET).....	30

3.4.3	Scanning Electron Microscopy (SEM).....	33
3.4.4	Thermogravimetric Analysis (TGA)	34
3.5	Reactor Setup	36
3.6	Glycerol Reforming	36
3.7	Fixed-Bed Reactor	37
4	RESULTS AND DISCUSSION	39
4.1	Introduction	39
4.2	Characterization of The Fresh Catalyst.....	39
4.2.1	Liquid N ₂ Physisorption by Brunauer Emmett Teller (BET).....	39
4.2.2	FESEM-EDX Imaging.....	41
4.2.3	X-Ray Diffraction (XRD).....	42
4.2.4	X -ray Photoelectron Spectroscopy (XPS).....	44
4.2.5	Thermo Gravimetric Analysis (TGA).....	51
4.3	Glycerol Reforming Reaction Studies	56
4.3.1	The Conversion of Main Reactant (glycerol).....	56
4.3.2	Effect of Reaction Temperature.....	57
5	CONCLUSIONS AND RECOMMENDATIONS	60
5.1	Conclusions	60
5.2	Recommendations	61
	REFERENCES.....	63
	APPENDICES	71

LIST OF FIGURES

Figure 2.1: Equilibrium Constant of Reactions Involving In Glycerol – CO ₂ Reaction at Different Temperatures and Atmospheric Pressure	11
Figure 2.2: Moles of Carbon Dioxide as a Function of CGR and Temperature at Atmospheric Pressure, $n^0(\text{C}_3\text{H}_8\text{O}_3) = 1\text{Mol}$	12
Figure 2.3: Moles of Hydrogen and Synthesis Gas Produced at Selected Pressures and CGR = 1, $n^0(\text{C}_3\text{H}_8\text{O}_3) = 1\text{ Mol}$	13
Figure 2.4: Moles of Hydrogen as a Function of CGR and Temperature at atmospheric Pressure, $n^0(\text{C}_3\text{H}_8\text{O}_3) = 1\text{ Mol}$	14
Figure 2.5: Moles of Carbon Monoxide as a Function of CGR and Temperature at Atmospheric Pressure, $n^0(\text{C}_3\text{H}_8\text{O}_3) = 1\text{ Mol}$	14
Figure 2.6: Proposed catalyst deactivation by sulphur poisoning mechanism during steam reforming (Satish L. Lakhapatri and Martin A. Abraham, 2011)	23
Figure 2.7: Models for crystalline growth due to sintering by movements of atoms A: migration; A': volatilization; B: migration of particles (M. Baerns, 2011)	24
Figure 3.1: Rigaku Miniflex II XRD	29
Figure 3.2: XRD Diffraction Line	30
Figure 3.3: IUPAC Classification of Adsorption Isotherms (ISO 9277, 2010)	31
Figure 3.4: Thermo-Scientific Surfer BET	32
Figure 3.5: Schematic diagram of FESEM.....	34
Figure 3.6: Weight Percent Loss against Temperature from TGA	35
Figure 3.7: Thermogravimetric Analysis Q500.....	35
Figure 3.8: Glycerol Reforming System	37
Figure 3.9: Schematic diagram of the Tubular Reactor for Glycerol Reforming	38
Figure 4.1: Isotherm plot for 3 wt% Ce-Ni/MgO.....	39

Figure 4.2: Isotherm plot for of 5 wt% Ce-Ni/MgO catalyst.....	40
Figure 4.3: SEM image of 5 wt% Ce-promoted Ni/MgO catalyst	41
Figure 4.4: EDX graph of 5 wt% Ce-promoted Ni/MgO catalyst	42
Figure 4.5: XRD patterns for 5 wt% Ce-promoted Ni/MgO catalyst	43
Figure 4.6: XP spectra of (a) Ni2p (b) Mg1s (c) O1s of fresh Ni/MgO catalyst	45
Figure 4.7: XP spectra of (a) Ni2p (b) Mg1s (c) O1s (d) Ce3d of fresh 3wt% CeNi/MgO catalyst	48
Figure 4.8: XP spectra of (a) Ni2p (b) Mg1s (c) O1s (d) Ce3d of fresh 5wt% Ce-Ni/MgO catalyst	50
Figure 4.9: Graph of derivative weight versus peak temperature for Ni/MgO catalyst at the heating ramp of 10°C/min.....	52
Figure 4.10: Graph of derivative weight versus peak temperature for 5wt% Ce-Ni/MgO catalyst for the heating ramp of 10°C/min.....	52
Figure 4.11: Graph of derivative weight versus peak temperature for 5wt% Ce-Ni/MgO catalyst for the heating ramp of 15 °C/min.....	53
Figure 4.12: Graph of derivative weight versus peak temperature for 5wt% Ce-Ni/MgO catalyst for the heating ramp of 20 °C/min	54
Figure 4.13: Plot of Kissinger model for two different catalysts	55
Figure 4.14: Plot of glycerol conversion, X_G vs flow ratios at (700 °C, 1 atm) for the first and second hours	56
Figure 4.15: Plot of glycerol conversion, X_G vs flow ratios at (750 °C, 1 atm) for the first and second hours	57
Figure 4.16: Plot of various rates of formation of each component for the first hour of the reaction	58
Figure 4.17: Plot of various rates of formation of each component for the second hour of the reaction	59

LIST OF TABLES

Table 2.1: Reactions in CO ₂ reforming of glycerol (Wang et al., 2009).....	10
Table 2.2: Summary of H ₂ Production with Noble Metals	17
Table 2.3: Mechanisms of Catalyst Deactivation (Bartholomew, 2001).....	20
Table 3.1: List of chemical and its purity	25
Table 3.2: List of Gases and their Respective Application	26
Table 3.3: Composition of Glycerol Used	26
Table 3.4: Functions of Used Equipment	27
Table 4.1: BET specific surface area, pore volume and pore diameter of the catalyst samples	40
Table 4.2: Summary of values of 2-theta, intensity, inter plane distance of crystal (d-spacing) and crystallite size for the diffraction peaks	43
Table 4.3: Binding energies of each element in fresh Ni/MgO catalyst and their corresponding count per unit second	46
Table 4.4: Binding energies of each element in fresh 3wt% Ce-Ni/MgO catalyst and their corresponding counts per unit second	48
Table 4.5: Binding energies of each element in fresh 5wt% Ce-Ni/MgO catalyst and their corresponding counts per unit second	51
Table 4.6: Results of the maximum peak temperature for two non-calcined catalyst samples at three different heating ramps	54
Table 4.7: Activation energy of catalyst samples.....	55

LIST OF SYMBOLS

P	gas pressure
P_s	saturation pressure of the adsorbate gas
V	volume of gas adsorbed
V_m	volume of gas adsorbed corresponding to monolayer coverage
c	a characteristic constant of the adsorbate
S_A	surface area of solid
a_m	average area occupied by a molecule
n_m	monolayer capacity of adsorbate
V_{liq}	volume of liquid N_2
V_{ads}	volume of nitrogen adsorbed
P_a	ambient pressure
r_k	Kelvin radius of the pore
γ	surface tension
E_k	kinetic energy
h	Planck's constant
ν	frequency
E_b	binding energy

Greek

ϕ	work function of spectrometer
λ	wavelength of X-ray beam
θ	angle of incidence
β_d	true line width at half maximum intensity
β_{ob}	observed width at half maximum intensity
β_{inst}	instrumental line width by standard

LIST OF ABBREVIATIONS

BET	Brunauer-Emmett-Teller
XRD	X-ray Diffraction
XPS	X-ray Photoelectron Spectroscopy
FESEM	Field Emission Scanning Electron Microscopy
EDX	Energy Disperse X-ray
TGA	Thermogravimetric analysis
POR	Partial Oxidation Reforming

CHAPTER 1

INTRODUCTION

1.1 Background

The demand for the hydrocarbon based compound as primary source of fuel has been on the rise in particular among the developing countries. This has led to unsustainable, uncontrolled exploration and exploitation of the non-renewable fossil fuel in order to support the industrial needs of the nation. Consequently, it causes the dwindling of petroleum reserves and inflicts severe environmental pollution as well as an excessive emission of greenhouse gases (CO_2 and CH_4). In replacement, glycerol (a bio-waste generated from biodiesel production) has been touted as a promising bio-hydrogen precursor via steam reforming route. Alternatively, dry (CO_2)-reforming of glycerol may provide another reforming route.

Hydrogen (H_2) has been considered as energy of future to substitute fossil fuel utilization. The increasing demand for H_2 for industrial and residential markets will provide a quantum leap towards hydrogen economy. H_2 is currently produced from hydrocarbon reforming (i.e. natural gas and petroleum) and electrolysis processes. Unfortunately, CO_2 produced by fossil fuel steam reforming has contributed to greenhouse effect. Therefore, new processes which are more environmentally friendly and economical for hydrogen production are clearly required. Glycerol ($\text{C}_3\text{H}_8\text{O}_3$), which is a byproduct of biodiesel production via alcohol trans-esterification of vegetable oils (triglycerides) has been considered as an excellent candidate for H_2 production. The $\text{C}_3\text{H}_8\text{O}_3$ utilization to produce H_2 or synthesis gas could potentially reduce the production costs of biodiesel.

Synthesis gas is a fuel gas mixture consists of carbon monoxide and hydrogen vital valuable feedstock in the downstream petrochemical industries, production of ammonia, methanol and etc. Furthermore, renewable energy has become a special interest in

nowadays society since the demand for energy resources increases rapidly. Synthesis gas plays a significant role in resolving the above mentioned issues. Synthesis gas can be used as an energy source for power plants generation. Besides, a wide range of synthetic products can be produced from the synthesis gas like clothes, solvents and fuels. Thus, it commands a high demand in the industry. In particular, synthesis gas is an important ingredient for major chemical intermediate in chemical processes for the synthesis of several fuels and chemicals (Wang et al., 2009).

As aforementioned, synthesis gas can be produced from natural gas, petroleum and its derivatives, biomass and coal via many routes. One of them is through the dry reforming of biomass such as glycerol. Significantly, glycerol reforming with CO₂ could be an attractive process although little is known about it. Since the bio-derived glycerol is considered to be renewable and CO₂-neutral, therefore by convention it will not contribute to the greenhouse effect. Secondly, glycerol dry reforming will convert CO₂ into synthesis gas or high value-added inert carbon and remove it from the carbon biosphere cycle (Wang et al., 2009).

Catalysts play a particular important role in this reaction. Normally it is comprised of a promoter, an active metal and also support. Promoter can strongly influence the physicochemical and catalytic property of the catalysts. Moreover, catalyst has a rich history of facilitating energy-efficient selective molecular transformations and contributes to 90% of chemical manufacturing processes and to more than 20% of all industrial products. In a post-petroleum era, catalysis will be central to overcoming the engineering and scientific barriers to economically feasible routes to biofuels and chemicals (Wilson et al, 2012). However, significantly previous studies have indicated that carbon deposition was the major performance-limiting factor for nickel (Ni) catalyst during glycerol steam reforming.

Therefore, in current research magnesium oxide (MgO)-supported Ni catalysts with cerium as promoter were prepared from wet co-impregnation method for the use in dry reforming of glycerol reaction. Thus, different loadings of cerium metal will be

incorporated in the catalyst formulation and tested with different flow rate and temperature in order to determine the optimum glycerol conversion that can be achieved. After that, the catalyst will be characterized with various techniques such as X-ray diffraction (XRD), Scanning Electron Microscopy (SEM), Brunauer Emmett Teller (BET) method and Thermogravimetric Analysis (TGA). The main purpose of performing these techniques is to study the physicochemical properties of catalysts.

1.2 Problem Statements

In spite of the great benefits which can be gained from H₂ gas production via reforming method, there are still many areas of uncertainty and these problems need to be solved before this application can be proceed commercially. There are also several issues or motivations behind the proposition for the current research that need a serious attention from researcher to ensure that this new technology is feasible in industry. Below are some issues that faced by most of the researchers:

- The current commercialized CH₄ steam reforming reactions with Ni based catalyst is not able to achieve conversion over 80% unless in extreme temperature conditions (> 800 °C).
- The thermodynamic, kinetics and characterization of glycerol dry reforming are not known as all prior published works are related to glycerol steam reforming.
- Carbon deposition behavior that leads to catalyst deactivation for most of the carbon containing reactants in particular glycerol is not well studied.
- Commercial process for syngas production by steam reforming leads to CO₂ formation which is not environmental friendly because CO₂ is a greenhouse agent.

1.3 Objectives

The current research aims to synthesize magnesium oxide-supported nickel catalyst promoted with cerium for the application in speeding up H₂ production via glycerol reforming.

1.4 Scopes

In order to achieve the aforementioned objective, the following scopes have been identified:

- I. To prepare Ce-Ni/MgO catalyst with the 3% loadings of Ce via co-impregnation method.
- II. To characterize the catalyst with various techniques such as:
 - X-ray diffraction (XRD) for crystallinity.
 - Scanning Electron Microscopy (SEM) for surface morphology.
 - Brunauer Emmett Teller (BET) method for surface area.
 - Thermogravimetric Analysis (TGA) for measuring of weight changes of solid samples using.
- III. To study the glycerol reforming reaction in a fixed bed reactor at 1 atm and reaction temperatures of 650 to 750°C.

CHAPTER 2

LITERATURE REVIEW

2.1 Introduction

Glycerol (also known as glycerine) is a by-product of biodiesel production process. Biofuels like ethanol and biodiesel are gaining significance due to the consistent decline in fossil fuels such as oil and natural gas reserves globally. Glycerol will be abundantly available as a by-product in lieu of the commercialization of biodiesel production. This has prompted researchers to find ways for utilization of glycerol to valuable products. Researchers working in the field of hydrogen and syngas production have now started focusing on the use of glycerol for hydrogen and syngas production by various techniques (Kale & Kulkarni, 2010).

Chemically, biodiesel is derived from fats and oils via trans-esterification method. Fats and oils are esters of the tri-alcohol, also commonly called triglycerides. This hydrolysis reaction produces glycerol and fatty acids, which are carboxylic acids derived from fats and oils. In the fatty acids, R represents groups of carbon and hydrogen atoms in which the carbon atoms are attached to each other in an unbranched chain. The reaction of the triglyceride in the reactor is the hydrolysis of the ester groups as shown in equation below:



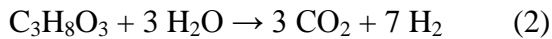
The bio-derived glycerol can be converted to synthesis gas via dry reforming and then used in Fischer-Tropsch synthesis (FTS), which can produce a large variety of hydrocarbons ranging from light gases to heavy wax. Liquid fuels from this biomass material provide renewable routes for fuel production (Wang et al., 2009). Synthesis gas is a major ingredient for many downstream petrochemical processes. Conventional production of syngas is via natural gas steam reforming. However, fossil hydrocarbons

resources are decreasing in the face of growing demand from developing countries; consequently resulting in a spike to energy price.

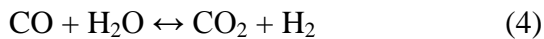
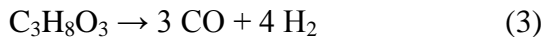
In this ensuing section, previous studies related to the reforming reaction, research catalysts, as well as catalyst deactivation phenomenon are presented.

2.2 Steam Reforming Reaction of Glycerol

Generally, glycerol can be converted into syngas by steam reforming process according to the follow reaction:



This overall reaction can be written as two separate reactions, viz. glycerol decomposition to hydrogen and carbon monoxide (Equation (2)) followed by water-gas shift reaction (Equation (3)):

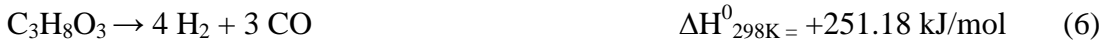


Cichy & Borowiecki (2008) stated that many catalytic systems used for glycerol steam reforming can be grouped under metals such as Ru, Rh, Ir, Pd, Pt, and Co. In addition, different supports were also used such as CeO₂, Al₂O₃, MgO, TiO₂ and ZrO₂. The most investigated catalysts are those based on Ni. Literature review shows that the addition of promoters to the nickel catalysts has improved their properties such as resistance to coking (K, Mo) and thermal stability (La, Ce). The researches on steam reforming with supported nickel as the catalyst have identified that it not only economical but also perform high steam reforming (Sanchez et al., 2010). Actually, the nickel catalyst has been regularly utilized as catalyzed in petroleum and natural gas processing industry because of its low cost and with the supported nickel used in reforming process; it is believed that the glycerol steam reforming can be commercialized too instead of methane (Trimm et al., 2004). It is economical for country that is abundance with waste glycerol such as Malaysia. However, the main problem faced by steam reforming is its intense

endothermic reaction which requires a lot of energy within the steam reforming reactor and normally this reaction is suitable for large-scale productions only.

2.3 Dry Reforming Reaction of Glycerol

The carbon neutral reforming or dry reforming of glycerol is industrially beneficial compared to steam reforming method in syngas production with greenhouse gas CO₂ could convert into synthesis gas or high value-added inner carbon. Besides, Wang et al., 2009 found that with a temperature of 1000 K and CO₂ to glycerol ratio of 1, the production of synthesis gas reaches a maximum with (H₂:CO = 1) can be produced per mole of glycerol with CO₂ conversion of 33%. The main reaction of dry reforming process is shown on the following equation:



The Equation (6) is the glycerol decomposition to hydrogen or synthesis gas and carbon monoxide and followed by production of methane which is shown by Equation (6). It is believed that the reaction cannot be shifted by changing the molar ratio of reactants when equilibrium constant K_p is much larger than 1, whereas when K_p is approaches 1, the molar ratio of reactant impacts the reaction trend significantly. For a multi-reaction system, the optimized target product mainly depends on the reactions with high K_p . Equilibrium constants of Equation (6) are great enough for complete decomposition of glycerol (Wang et al., 2009). In contrast, many preliminary researches have been done by using simple hydrocarbon fuel such as methane to produce synthesis gas via dry reforming and many papers have been published on methane catalytic dry reforming while glycerol dry reforming is not yet much published (Gao et al., 2011). Hence, a lot of data is still remaining unknown for dry reforming using glycerol. However, there is an

important drawback from the dry reforming method that may lead to a higher rate of carbon deposition and cause catalyst deactivation via coking (Gallego et al., 2008).

2.4 Partial Oxidation Reforming

The syngas production which requires oxygen and hydrocarbon raw materials in the reaction is referred as partial oxidation. This reaction is illustrated in the equation (8). The partial oxidation process is determined to have potential to replace the steam reforming method which is highly endothermic. This process usually requires external cooling as it is highly exothermic while operating at a higher temperature than the steam reforming method (Lucrecio, 2007). The carbon deposition and sulphur poisoning issues in syngas production process can be overcome by using high temperature in partial oxidation method. Moreover, the partial oxidation process for syngas production does not require water supply system like in steam reforming method and hence, reducing the production cost.

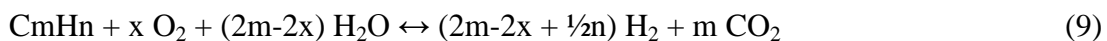


As the partial oxidation method for syngas production is characterized as an exothermic reaction, its reactor can be started faster than the steam reforming reactor. Therefore, the partial oxidation reactor does not require heat transfer optimization which can be designed to be lighter and in a more compacted size. In other words, the partial oxidation method is suitable to be used in a smaller system. Besides that as the partial oxidation reaction is exothermic, adiabatic reactor can be used for methane partial oxidation process. It has been determined that the stoichiometric of the partial oxidation reaction according to the equation (4) has a product molar ratio of H₂/CO equals two. This product molar ratio is suitable for Fisher-Tropsch and methanol synthesis. Moreover, the high operating temperature of partial oxidation process is favourable to be used for the solid oxide fuel cells as it will hinder the CO poisoning of the fuel cells. Apart from that, partial oxidation process is also a catalytic synthesis process and supported nickel is the catalyst that has been widely used for the

process, same as steam reforming method because of its high catalytic activity and low cost. Anyway, it has been reported that the amount of hydrogen gas that is generated by partial oxidation reaction is lower than the steam reforming reaction. Besides, the overall energy consumption and production cost of the partial oxidation reaction will be higher than steam reforming method. Hence, the partial oxidation method is still not the best method for syngas production in industry.

2.5 Auto-thermal Reforming

It has been reported that steam reforming method produces higher efficient and yield of synthesis gas but is unsuitable for portable unit application because of its high endothermic reaction. On the other hand, partial oxidation has lower yield of hydrogen gas and its operating system is too high to be commercialized. Anyway, it is suitable as if the system is small. Meanwhile, auto-thermal reforming is the method that uses the combination of partial oxidation method and steam reforming method which is shown in equation (9) (Nilsson et al., 2009). Hence, the auto-thermal reforming process possesses higher synthesis gas production efficiency and simple system design which require lower investment than other processes. The main mechanism of the auto-thermal reforming method is also showed by equation (9) below.



The 'x' is the variable that represents the oxygen-to-fuel ratio which is used as the auto-thermal reforming's heat transfer controller. For instance, the overall reaction will be partial oxidation dominant and become more exothermic when the value of x is higher. Meanwhile, the overall reaction will be steam reforming dominant and become more endothermic when the value of x is lower. In other words, the x value is used to adjust the overall reaction either towards exothermic or endothermic, depends to requirement. Anyway it has been reported that the overall reaction will be controlled to be a bit more towards exothermic to enable self-sustenance of the reactor (Kang & Bae, 2006). Therefore unlike steam reforming, auto-thermal reforming does not

require heat from outer source and its operating temperature is normally lower than the partial oxidation method for synthesis gas production. Then, another ratio which can be controlled is the steam-to-fuel ratio for different product composition. In order to produce higher hydrogen yield, the steam-to-fuel should be higher. The addition of steam in the reaction helps in its water-gas-shift mechanism and leads to higher hydrogen production while additional of oxygen can lower the coke formation possibility and make the reaction faster. It is determined that although auto-thermal reforming method is the combination of partial oxidation method and steam reforming method, the reactions take place in sequence, where partial oxidation reaction occurs following by the steam reforming reaction and, so the auto-thermal reforming reaction can be initiated in a fast rate (Lim et al., 2009). In other words, the auto-thermal reforming method contains the advantages from both steam reforming and partial oxidation method (Escritori et al., 2009). However it is reported that, the concentration of hydrogen within the production from the auto-thermal reforming method is just in between partial oxidation and steam reforming method, meaning that it still lower than the gas generation from steam reforming.

2.6 Thermodynamics Analysis of Reactions in Glycerol Dry Reforming

Table 2.1 below show the main reactions which may occur in CO₂ reforming of glycerol.

Table 2.1: Reactions in CO₂ reforming of glycerol (Wang et al., 2009)

Possible reactions	ΔH_{298K} (kJ/mol)	No. of Equation
$C_3H_8O_3 \leftrightarrow 4H_2 + 3CO$	251.18	(11)
$CO + 3H_2 \leftrightarrow CH_4 + H_2O$	-206.11	(12)
$CO_2 + 4H_2 \leftrightarrow CH_4 + 2H_2O$	-164.94	(13)
$CO_2 + CH_4 \leftrightarrow 2H_2 + 2CO$	247.28	(14)
$CO + H_2O \leftrightarrow H_2 + CO_2$	-41.17	(15)
$C + H_2O \leftrightarrow H_2 + CO$	131.26	(16)



Figure 2.1 shows the equilibrium constant of reactions involving in glycerol – CO₂ reaction at different temperatures and atmospheric pressure.

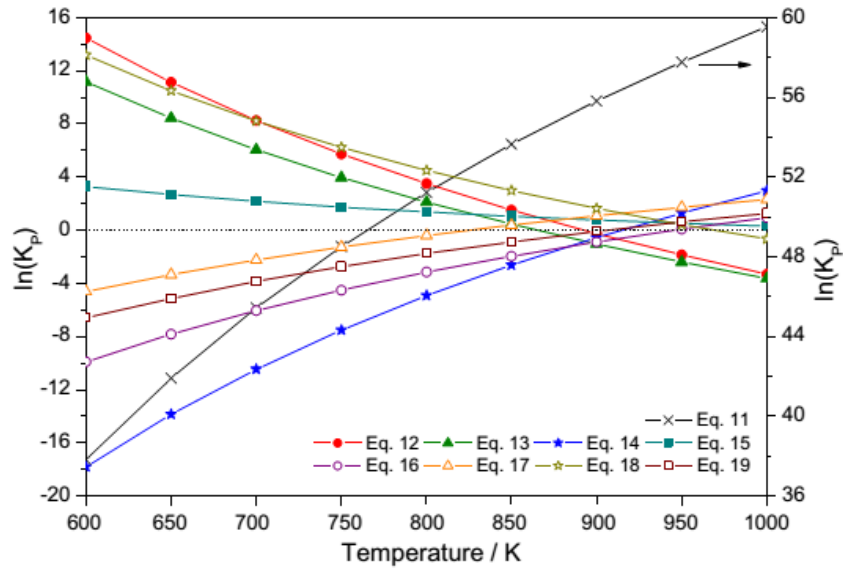


Figure 2.1: Equilibrium Constant of Reactions Involving In Glycerol – CO₂ Reaction at Different Temperatures and Atmospheric Pressure

2.6.1 Carbon Dioxide Conversion

As aforementioned, one of important advantages from glycerol dry reforming is that CO₂ can be converted into synthesis gas or sequestered and removed from the carbon biosphere cycle. Therefore, the conversion of CO₂ needs to be considered and discussed. Figure 2.2 shows moles of CO₂ versus temperature at different CGRs. Moles of CO₂ at equilibrium reach a maximum between 750 K and 825 K regardless of CGRs. This can be

ascribed to the reformation of CO_2 with CH_4 . High temperature favours the conversion of CO_2 . For CGRs 1–5, the conversion of CO_2 reaches 30–39% over 950 K. While for other CGRs considered in this work, the moles of CO_2 at equilibrium are more than initial input quantities (Wang et al., 2009).

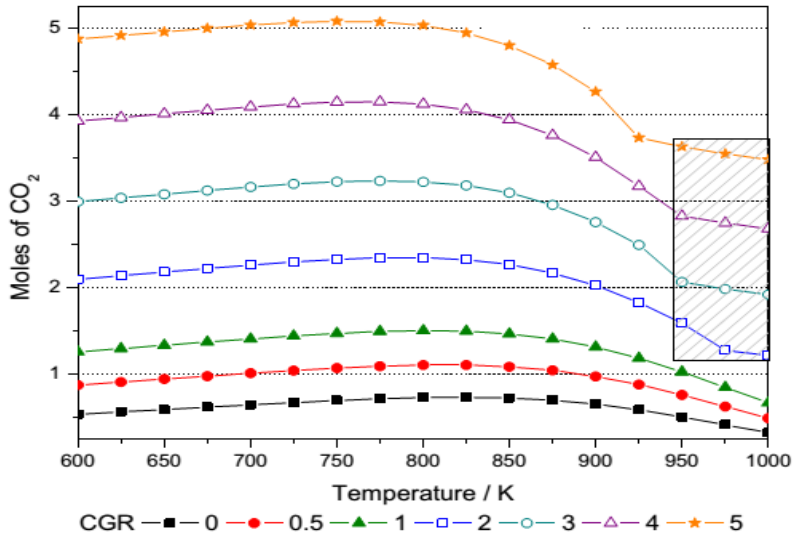


Figure 2.2: Moles of Carbon Dioxide as a Function of CGR and Temperature at Atmospheric Pressure, $n^0(\text{C}_3\text{H}_8\text{O}_3) = 1 \text{ Mol}$.

2.6.2 Hydrogen and Synthesis Gas Production

Figure 2.3 depicts the production of hydrogen and synthesis gas at different temperatures and pressures. Briefly, the amount of hydrogen and synthesis gas produced decreases with the increase in pressure. Therefore, Wang and his partners selected atmospheric pressure as the best one with respect to hydrogen and synthesis gas production all through following discussions. As can be seen from Figure 2.4, moles of hydrogen increase with increasing temperature all the way when CGR is < 1 , whereas with CGR higher than 1, the number of moles of hydrogen increases with increasing temperature, goes through a maximum around 925–975 K, and then decreases at higher temperatures. Moles of

hydrogen decrease together with CO₂ over temperatures at which hydrogen production maximizes, while moles of water and CO increase. This probably can be explained by reaction (15). The effect of CGR on hydrogen production is not significant when it is < 2, but high CGRs reduce the capacity of hydrogen production when temperature is higher than 925 K. More than 3 moles of hydrogen can be generated at CGRs between 0 and 1 over 975 K. The amount of hydrogen produced in glycerol dry reforming is less than those reported previously (Wang XD et al., 2008; Adhikari et al., 2007). The K_ps associated with reactions involving H₂ are plotted in Figure 2.1. It can be seen that reaction (11) proceeds more easily with the entire considered temperature range. The reversion of reaction (14) is feasible below 800 K and then limited by equilibrium. Reactions (12), (13), (16), and (19) are affected by equilibrium limitations when temperature is higher than 700 K. Reactions (15) and (17) are limited within the whole investigated temperature range.

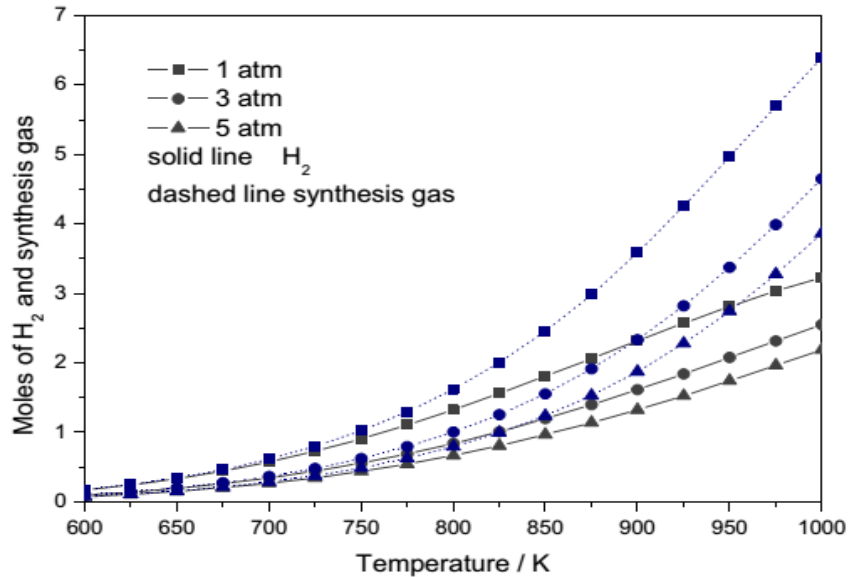


Figure 2.3: Moles of Hydrogen and Synthesis Gas Produced at Selected Pressures and
 $\text{CGR} = 1, n^0(\text{C}_3\text{H}_8\text{O}_3) = 1 \text{ Mol}$

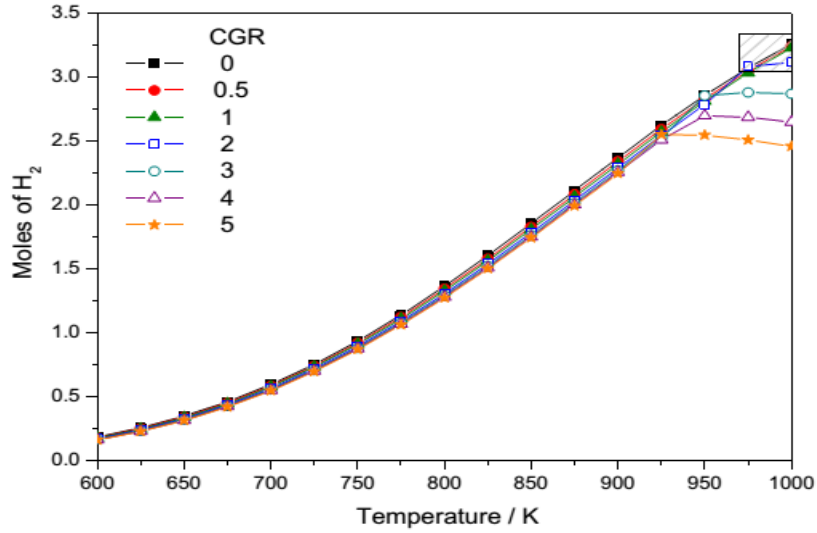


Figure 2.4: Moles of Hydrogen as a Function of CGR and Temperature at atmospheric Pressure, $n^0(\text{C}_3\text{H}_8\text{O}_3) = 1 \text{ Mol}$

Figure 2.5 shows moles of CO as a function of CGR and temperature at atmospheric pressure.

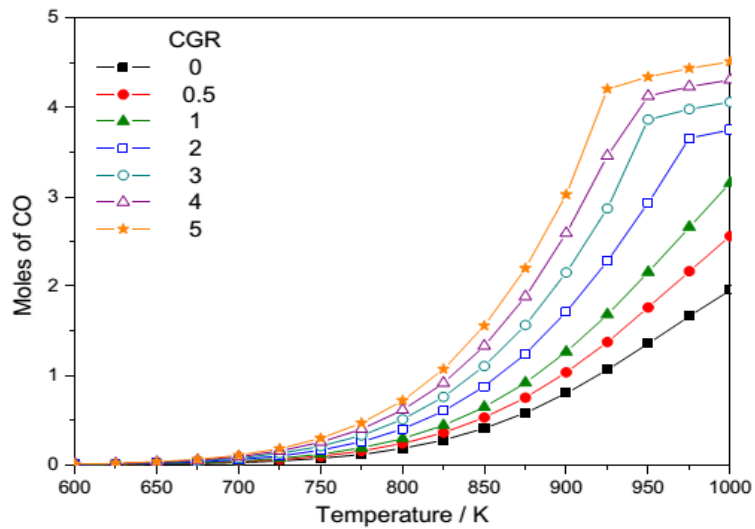


Figure 2.5: Moles of Carbon Monoxide as a Function of CGR and Temperature At Atmospheric Pressure, $n^0(\text{C}_3\text{H}_8\text{O}_3) = 1 \text{ Mol}$.

High CGR and temperature favour CO production. High concentration of CO in equilibrium is not feasible for further application of hydrogen in fuel cell. But it provides a good opportunity for synthesis gas production. The required properties of synthesis gas vary with different synthetic reaction. For methanol synthesis, the desirable composition of synthesis gas is a H₂/CO ratio of about 2 (Simonetti et al., 2007). The ratios equal to 1.7 and 2.15 are suitable for FTS (Dry, M.E, 2002). Furthermore, a H₂/CO ratio of 1 is desirable for direct favour downstream synthesis of different fuels and chemicals (Wang et al., 2009).

2.7 Catalyst Used For Reforming Reaction

Nowadays, there are more than ten kinds of single metals and a large number of alloys have been used for the dry reforming reactions. Among them, Ni, Co, Rh, and Pt are the most reported catalysts. The catalyst which is mostly used in the researches for chemical reaction is nickel based. This is due to nickel possesses higher reactivity and its cost is lower than the noble metal catalysts. Anyway, nickel based catalyst can be easily deactivated by carbon deposition. Hence, many attentions have been put on enhancing the stability and activity of the nickel catalyst to reduce the carbon deactivation issue such as choosing a suitable syngas generation method, type of catalyst support or adding promoters. In this research, Cerium - one of the rare-earth types has been used as the catalyst promoter. Furthermore, the catalyst which is made by nickel and supported by magnesium oxide has been widely used in various researches. In addition, Ni catalyst is widely used because of its low cost and high availability and to its high activity for C-C bond cleavage. On the other hand, γ -Al₂O₃ was used as a main support and, moreover, it was modified with La₂O₃ or CeO₂ for several reasons. According to the literature, La₂O₃ is particularly suitable as a γ -Al₂O₃ modifier due to its effectiveness in preventing sintering and improving thermal resistance at high temperatures. This oxide is also able to gasify the coke through the formation of La₂O₂CO₃ oxy-carbonate species. Moreover, La₂O₃-based catalysts show high activity and selectivity toward H₂ production during the reforming reaction of glycerol. While for the CeO₂, there were two reasons for modifying

the support with this oxide: first, because it performs well as a support for Ni catalysts, and secondly due to the addition of CeO₂ to Pt catalysts improves the activity of this metal in Water-Gas-Shift reaction (El Doukkali et al., 2012). It is believed that when adsorption and CO₂ activation is increased, the gasification of the surface carbons can occur in a faster rate and prevent the inactive carbon decomposition on the surface of the catalyst. Besides, many basic components have been used to be catalyst supporter as an effort to make the catalyst more in alkaline. Moreover, rare earth metal such as lanthanum has been widely used to increase the alkalinity (Juan et al., 2006). It has also been determined that potassium (K)-modified alumina supported nickel catalyst can cause a decrease of carbon deposition on the surface of the catalyst. Potassium improves the metal support interaction; in addition some of the potassium can move from the support to the metal surface to neutralize the fraction of the active sites (Luna et al., 2008). In spite of that, inactive carbon formation is induced when component such as calcium or manganese is added into the catalyst and reduces the catalytic activity (Luna et al., 2008). However by using a suitable amount of basic oxide, MgO and CaO, catalytic performance of the alumina supported nickel catalyst can be improved as a strong metal-support attachment can control the carbon deposition on the surface of the catalyst during dry reforming method (Roh et al., 2008). On the other hand, A few researches have been brought out to produce synthesis gas via methane dry reforming using noble metal as catalyst such as Rh, Ir, Ru and Pt. It has been determined that the dry reforming process occurs easily with the noble metal catalyst. Anyway, the synthesis gas production using noble metal as catalyst has failed to be commercialized because the cost of the noble metal is too high and low availability. Then researchers have found other component to replace the noble metal as catalyst for synthesis gas production. According to previous researches, it has been determined that nickel has similar catalytic reactivity with the noble metals after comparison has been made for both type of metals but the main drawback is, the nickel catalyst is easier to have carbon deposition problem (Nielsen & Hansen, 1993). However, further research has been brought by using noble metal as promoter for nickel based catalyst because only a small amount of noble metal is required to be the promoter and it has been determined that the noble metal promoter can lead to have the combination

benefits from both nickel and noble metal; higher activity and lower carbon formation rate during the dry reforming of methane (Hou and Yashima, 2003). Table 2.2 below depicts the H₂ production with noble metals as reforming catalyst.

Table 2.2: Summary of H₂ Production with Noble Metals

Reforming Method	Catalyst	Hydro-carbon	Reaction Temp. (K)	Reaction Pressure	Sources	Effect of Noble Metal
Dry	RhNi/ZrO, Rh/ZrO ₂ , Ni/ ZrO ₂	Methane	823-973	1 atm	Irusta et al., 2002	-0.2% Rh/ZrO ₂ : most stable, active @ 823K. Just little carbon formed @ 973K.
Dry	RhNi/Al ₂ O ₃ , Rh-Ni/BN	Methane	298-973	1 atm	Wu & Chou, 2003	-Rh-Ni/BN improved H ₂ production. Coke formation reduced.
Dry	Pt/Al ₂ O ₃ , Pt/TiO ₂ , Pt/ZrO	Methane 1 atm	875	1 atm	Bitter et al., 1996	-Pt/ZrO ₂ inhibited coking formation. Highest CO ₂ conversion is 32% with Pt/Al ₂ O ₃
Supercritical Water	Ru/Al ₂ O ₃	Glycerol	973-1073	1atm	Byrd et al., 2008	-H ₂ increased when temperature increased. Lower residence time reduced CH ₄ formation. Activation energy= 55.9 kJ/mol

Steam	Ir/CeO ₂ , Ir/CeO ₂ - PrO	Ethanol	673-923	1 atm	Wang et al., 2011	-Ir/CeO ₂ -PrO ₂ catalyst is highly active and stable. Promoted redox property of oxide support.
Steam	Cu/Nb ₂ O ₅ , RuCu/NbO ₅ , PdCu/Nb ₂ O ₅	Ethanol	300	1 atm	Alonso et al., 2009	-Ru & Pd promoted catalyst significantly enhance H ₂ production, ethanol conversion & carbon deposition resistance.
Steam	Pt/SiO ₂ , Pt/Al ₂ O ₃ , Pt/ZrO	Glycerol	450	1 atm	Pompeo et al., 2010	-Pt/SiO ₂ promotes dehydrogenation reaction & C-C cleavage. High stability.

2.8 Catalyst preparation methods for reforming reaction

There are several preparation methods that used to develop the catalyst for reforming reaction. However, it is believed that the physical characteristics of the developed catalyst will be influenced by the preparation method. Therefore, an appropriate catalyst preparation should be chosen based on the physical properties of the expected catalyst so that the catalytic activity can be enhanced. Besides, the shape of the catalyst also will contribute to its performances. In 2012, L.F. Bobadilla and his researchers have made the comparison between the structured catalyst prepared and the conventional catalyst (spherical pellets and powder), they found that both catalysts showed the same activity and selectivity for the first hour, but the conventional catalysts were rapidly deactivated.

The structured catalyst was not deactivated after 50 h of the reaction. Moreover, the most common catalyst preparation method is by impregnation of metal salt in aqueous solution onto a support material such as MgO to nickel catalyst. There is another practical method which is co-precipitation also widely used in catalyst preparation. Through this method, the metal salt solutions is mixed at constant pH value and then precipitated into desired products. After that, the developed catalysts obtained will be calcined at certain temperature corresponding to the physical properties of the catalyst in order to remove the carbon deposited on the catalyst surface. In addition, an influence of the calcination temperature on both catalyst characteristics and performance was found recently. For example, increasing the calcination temperature from 700 to 900 °C resulted in a reduction of both surface area and hydrogen concentration in the produced gas (Paula H. Blanco, 2014).

2.9 Catalyst Deactivation

The main problem that plagues catalytic process is attributed to catalyst deactivation. For good catalytic process, the catalyst must be active, selective, durable, and tolerant to coking and sulphur poisoning (Liu, 2012). Hence, many methods to reduce the catalyst deactivation rate have been tested, i.e. appropriate selection of active metals and also support materials. Therefore, this is one of the most challenging attempts in order to develop the catalytic fuel processing. Thus, there is a considerable motivation to understand the mechanisms behind catalyst deactivation so that possible steps to slow down the process can be implemented. Table 2.3 below shows six different mechanisms of catalyst deactivation.

Table 2.3: Mechanisms of Catalyst Deactivation (Bartholomew, 2001)

Mechanism	Type	Brief Definition/Description
Poisoning	Chemical	Strong chemisorption of species on catalytic sites,

		thereby blocking sites for catalytic reaction
Fouling	Mechanical	Physical deposition of species from fluid phase onto the catalytic surface and in catalyst pores
Thermal degradation	Thermal	Thermally induced loss of catalytic surface area, support area, and active phase-support reactions
Vapor formation	Chemical	Reaction of gas with catalyst phase to produce volatile compound
Vapor-solid & solid-solid reaction	Chemical	Reaction of fluid, support, or promoter with catalytic phase to produce inactive phase
Attrition/Crushing	Mechanical	Loss of catalytic material due to the abrasion and internal surface area due to mechanical-induced crushing of the catalyst particle

2.9.1 Carbon Deposition

Hydrocarbon fuels contain components such as alkanes and aromatics. At a certain temperature and condition, alkanes and aromatics will crack or dissociate to form solid carbon and coke. Consequently, this will cause catalyst fouling on the catalysts. Nickel based catalyst is commonly deployed in many catalytic researches and even in commercialized hydrogen production due to its high catalytic activity, availability and low cost. Unfortunately, it has been found that nickel catalyst is prone to carbon deposition leading to catalyst deactivation (Lee et al., 2012). In contrast, noble metal catalyst is more resilient to carbon deactivation, but is more cost-prohibitive (Lemonidou et al., 1998). Hence, there is a strong will to overcome carbon deposition on the nickel based catalyst. However, this will be the most difficult challenge in catalytic hydrogen production industry. As methane is the simplest chemical molecule structure, it is used in many hydrogen gas production researches and even applied widely in industry (Seth, 2002; Dave, 2010). This is because, complex hydrocarbon fuels like glycerol, ethanol, ethanoic acid, diesel and gasoline possessing longer carbon chain and will lead to higher carbon formation rate when the carbon chain is cracked (Saunders & Kendall, 2002). However, researchers have started to try for a higher level of hydrogen production with higher hydrocarbons and determine for the methods to overcome the carbon deposition issue. Researchers have reported four main carbon formation mechanisms from the methane reforming process which include methane decomposes to hydrogen and carbon on the metal active sites; carbon atoms dissolve and diffuse into the metal bulk phase; carbon atoms segregate to form a grapheme layer; and carbon whiskers grow at the metal particles by stacking the grapheme layers (Kiyoshi et al., 2008).

2.9.2 Poisoning

Poisoning occurs when there is the strong chemisorption of species which is normally referred to sulphur present on catalyst, thus blocking active sites for catalytic reaction.

Sulphur will accumulate on the catalyst surface and accelerate the loss of the catalyst active sites because of the strong interaction between the active sites and sulphur (Cheng, 2011). Sulphur presents as a compound naturally. The most common sulphur compound in natural gas is hydrogen sulphide (H_2S). Besides, the longer chain hydrocarbon species such as gasoline and diesel would contain sulphur compound in a more complex form. In the industry, the catalysts used for reforming process will be deactivated by the sulphur compound and most probably the catalyst have to be replaced frequently, leading to a high cost production. According to Jiang et al., 2011, it is a good idea to desulphurize the hydrocarbon fuels before carry out the reforming process but there is another huge amount needed for desulphurization process. Therefore, direct reforming process is more feasible as it is still considered having a lower cost and more simple process compared to the desulphurization method. In other words, the reforming industry nowadays stills using a high cost process for hydrogen production and lead to expensive product (Wang, 1997; Babich & Moulijn, 2002). Therefore, the continuous research is still carried on in order to determine the best method to produce sulphur resistance catalyst. Thus, it is important to study the mechanism of sulphur poisoning. Several studies have been initiated to understand the mechanism of the sulphur poisoning process, to improve the sulphur tolerance, and to regenerate the reforming catalyst. It has been proposed that the mechanism of sulphur poisoning is very similar to that of the NO_x storage process. Under lean conditions, SO_2 is oxidized on the precious metal site and then reacts with the support and the NO_x storage component. Under rich conditions, sulphur containing species interact with the noble metal and sulphides, such as PtS , are formed (Czekaj, I et al., 2011). Figure 2.6 illustrate the concept of sulphur poisoning mechanism.

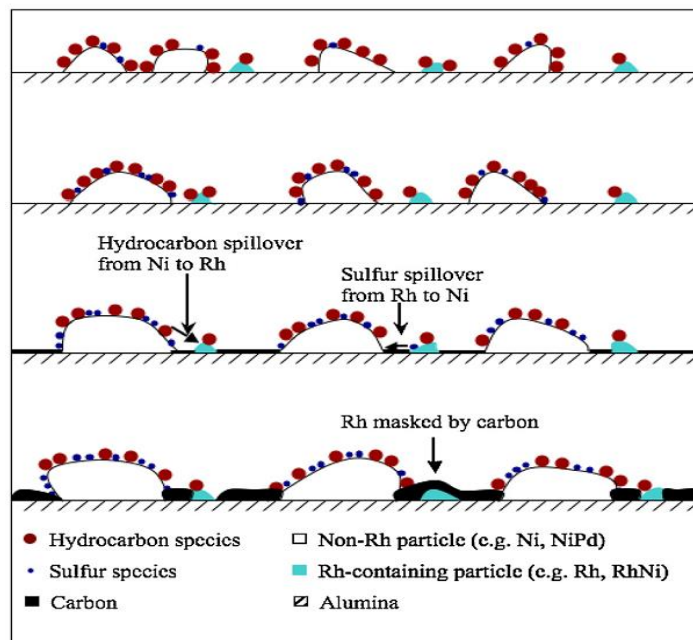


Figure 2.6: Proposed catalyst deactivation by sulphur poisoning mechanism during steam reforming (Satish L. Lakhapatri and Martin A. Abraham, 2011)

2.9.3 Catalyst Sintering

Sintering or aging is also one of the drawback that faced by reforming catalyst from the past to present. According to Jens Sehested et al., 2004, sintering of heterogeneous catalysts is often referred to as the loss of catalytic surface area due to growth of large particles at the expense of smaller particles. Sintering process is complex and may be influenced by many parameters such as sintering time, temperature, chemical environment, catalyst composition and structure, and support morphology. A good understanding of the sintering mechanism is necessary, both to predict the extent of deactivation by sintering and to design catalysts that maintain a high activity. Hence, there are several studies of sintering of Ni particles supported on a ceramic carrier are reported in the literature. The most important parameters are the sintering temperature and the composition of the gas over the catalyst. There is the evidence that increasing temperature and the presence of steam will accelerate the sintering process (C.H.

Bartholomew, 1993). Besides, high surface areas of the carrier will increase the stability toward sintering (J.T. Richardson et al., 1979). Three mechanisms for the metal particle growth have been proposed by Jens Sehested and his co-researchers which are particle migration, where entire crystallites migrate over the support followed by coalescence; Ostwald ripening (atom migration), where metal atoms emitted from one crystallite migrate over the support and are captured by another crystallite; and vapour transport between particles (at high temperatures). Figure 2.7 shows the models for crystalline growth due to sintering process.

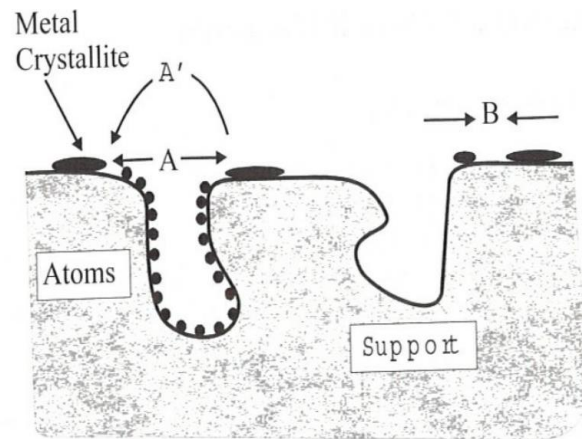


Figure 2.7: Models for crystalline growth due to sintering by movements of atoms A: migration; A': volatilization; B: migration of particles (M. Baerns, 2011)

CHAPTER 3

METHODOLOGY

3.1 Introduction

This section provides materials description, catalysts preparation, catalyst characterization and catalyst testing. Furthermore, the theoretical fundamentals and operational procedures of catalyst characterization instruments will also be discussed.

3.2 Materials

3.2.1 Chemicals for catalyst synthesis

The catalyst used in this experiment is Ce-promoted Ni/MgO catalyst. All the materials required for catalyst preparation such as cerium, nickel and magnesium oxide are supplied by Sigma-Aldrich Sdn. Bhd as listed in Table 3.1.

Table 3.1: List of chemical and its purity

Chemical	Purity
Cerium nitrate ($\text{Ce}(\text{NO}_3)_2$)	>98%
Nickel nitrate ($\text{Ni}(\text{NO}_3)_2$)	>98%
Magnesium oxide (MgO)	>98%

3.2.2 Gases

The gases employed in the research are supplied by Air Products. The list of grade and application of the gases are given in Table 3.2.

Table 3.2: List of Gases and their Respective Application

Gas	Purity/Concentration	Application
CO ₂	> 99.99%	Reactant
H ₂	> 99.99%	Catalyst reduction
Argon	> 99.99%	GC carrier gas/ Reactants diluent
N ₂ & He	> 99.99%	Diluent for H ₂ chemisorption & TPD analyses
Air	> 99.99%	Total carbon analysis & TGA

3.2.3 Glycerol

Analytical grade glycerol which is the main material for this research was purchased from Timur Network Malaysia Sdn. Bhd. The purchased glycerol is in liquid form and colourless. Its chemical composition is as listed in the Table 3.3.

Table 3.3: Composition of Glycerol Used

Component	Content
Assay	99.5%
Fatty Acids	0.05%
Water	0.45%

3.3 Catalysts Preparation

The catalyst is prepared using wet co-impregnation method. The aqueous precursor solutions of both nickel ($\text{Ni}(\text{NO}_3)_2$) and cerium ($\text{Ce}(\text{NO}_3)_2$) are impregnated together onto the MgO solid support with pre-determined concentration in order to obtain the fixed Ni loading of 20 wt% and Ce loading of 3 wt%. Then, the resulting slurry is allowed to be dried at temperature of 130 °C. After drying, the samples are calcined at 900°C.

3.4 Catalyst Characterization

It is important to determine the bulk and surface properties of the catalysts in order to investigate its performances. The characterization methods can be grouped into morphological, microscopic, spectroscopic and physicochemical methods. In this section, the fundamental theory and concepts of various characterization methods used in this research work will be described in detail. The summary for the function of the equipment involved in this research work is shown in Table 3.4.

Table 3.4: Functions of Used Equipment

EQUIPMENT	FUNCTION
BET	Specific surface area determination
XRD	Crystallinity, crystallite size and structure study
TGA	Online measurement of weight changes with temperature
EDX	Morphology and chemical composition determination
TPD	Measure the quantitative and

	qualitative aspects of desorbed species from solid sample
TPR	Study interaction between solid oxide metal and
TPO	Study carbon deposition

3.4.1 X-ray diffraction (XRD)

One of the characterization techniques involved in this study is X-ray diffraction (XRD) which is used to investigate the crystalline structure of the catalysts. X-ray powder diffraction (XRD) is a versatile, non-destructive rapid analytical technique which is mainly applied for phase identification of a crystallite. The information which can be retrieved from XRD is chemical composition, finely homogenized and average bulk composition as well as crystallographic structure (Dutrow & Clark, n.d.). In 1912, a scientist named Man von Laue has found that crystalline materials can perform as three-dimensional diffraction gratings for X-ray wavelengths which are similar to the crystal lattice's plane spacing. Therefore, XRD has been commonly adopted to determine the atomic spacing and crystal structures for material (Dutrow & Clark, n.d.). The particle size of the catalyst samples must be ground to less than 100 μm for XRD analysis. The solid samples are irradiated with nickel-filtered $\text{CuK}\alpha$ radiation with a wavelength (λ) of 1.542Å at 40mA and 45kV. The sample scanning will be carried out from 10° to 80° at the scanning rate of 4 min^{-1} by using Rigaku Miniflex II XRD.



Figure 3.1: Rigaku Miniflex II XRD

XRD technique requires the use of CuK radiation and monochromer graphite for analysis. Figure 3.1 illustrates the working principles of XRD where X-ray beam is directed onto the crystal surface and the diffracted line is reflected to a recorder for data collection. The mean size of crystallites can be calculated from the Scherrer equation (cf. equation (3.1)).

$$d = \frac{K\lambda}{\beta \cos\theta} \quad (3.1)$$

where

K = the shape factor (taken as 0.9)

λ = the X-ray wavelength

β = the line broadening at half the maximum intensity (FWHM) in radians

θ = the Bragg angle

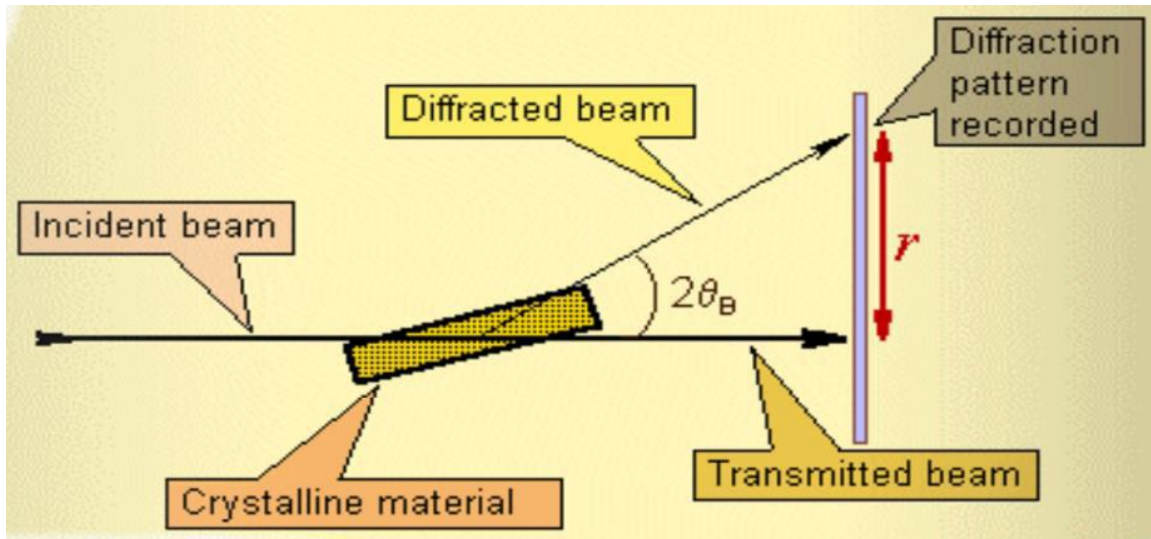


Figure 3.2: XRD Diffraction Line

3.4.2 Brunauer Emmett-Teller (BET)

The most common and effective procedure for determination of the surface area of solid materials is the Brunauer-Emmett-Teller (BET) method (Brunauer et al., 1938), which is an extension of the Langmuir's pioneer work (Langmuir, 1916) for monomolecular adsorption. Liquid N_2 physisorption method is commonly used to determine the specific surface area, average pore radius and pore volume of a porous solid sample such as catalysts (Hossain *et al.*, 2009). The parameters are measured from N_2 physisorption isotherms using the Brunauer-Emmett-Teller (BET) volumetric method (Natesakhawat *et al.*, 2005). The liquid N_2 adsorption-desorption isotherms are obtained at 77 K over the whole range of relative pressures. Before measurements, the samples have to be degassed at a certain temperature for overnight (Iriundo *et al.*, 2010). The isotherms obtained could reveal whether the structure is macroporous, mesoporous or microporous. Figure 3.1 shows that the BET technique is suitable for adsorption isotherms of type II (disperse, nonporous or macroporous solids), type IV (mesoporous solids, pore diameter between 2 nm and 50 nm) or a microporous materials which is a type I isotherms (ISO 9277, 2010).

The pore size in the range of 0 to 2 nm is referred as microporous, 2 to 50 nm is referred as mesoporous and pore size exceeding 50 nm represents macroporous (Léonard *et al.*, 2006).

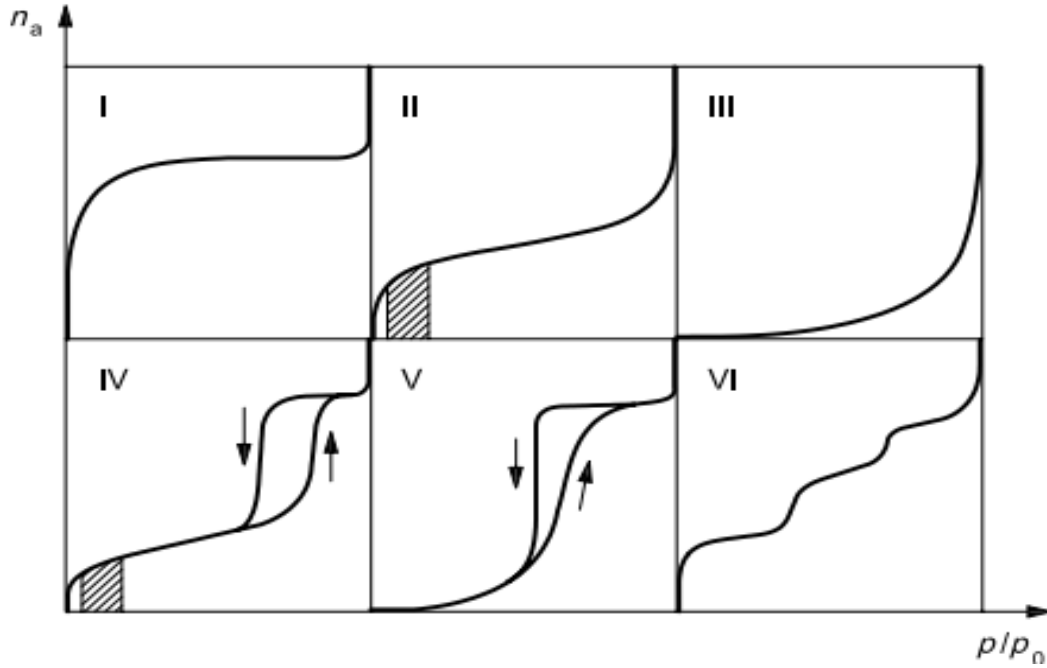


Figure 3.3: IUPAC Classification of Adsorption Isotherms (ISO 9277, 2010)

BET equation is derived for multilayer adsorption and based on the relationship between the volume of gas physically adsorbed and the total area of adsorbent, given by:

$$\frac{P}{V(P_s - P)} = \frac{1}{cV_m} + \frac{(c-1)P}{cV_m P_s} \quad (3.2)$$

where

P = gas pressure

P_s = saturation pressure of the adsorbate gas

V = volume of gas adsorbed

V_m = volume of gas adsorbed corresponding to monolayer coverage

c = a characteristic constant of the adsorbate

V_m and c may be calculated via the slope and intercept respectively from a linear plot of $P/V (P_s - P)$ against P/ P_s . The volume V_m , can then be converted to the number of molecules adsorbed by using the known value of cross-sectional area of the adsorbent gas molecule. Multi-point BET method is used to determine the total surface area, pore volume and pore size distribution of the sample by using Thermo Surfer from Thermo Scientific. BET Multipoint method is employed in the analysis. In order to analyse, solid catalyst sample (0.3-0.4 g) is weighed into the sample holder. Then it is degassed at 573 K for overnight to remove moisture and volatile impurities from the sample (Cheng *et al.*, 2011). Subsequently, the sample is transferred to the analyzer compartment for physical properties measurement at 77 K. Nitrogen gas with a cross-sectional area of 16.2\AA^2 is used as the adsorbate in the analysis. During the adsorption step, the data from the volume of the injected N_2 to the adsorbent and the measured equilibrium pressure is applied to construct the adsorption isotherm. Similarly, desorption isotherm is constructed by the quantity of the N_2 removed from the sample. In the current work, BET analysis is performed using Thermo-Scientific Surfer available as illustrated in Figure 3.4.



Figure 3.4: Thermo-Scientific Surfer BET

3.4.3 Scanning electron microscopy (SEM)

SEM uses a focused beam of high-energy electrons to generate a variety of signals at the surface of solid specimens. The signals that derive from electron sample interactions reveal the information of morphology (size and shape), topography (surface features), and crystallographic (atomic arrangement) of the catalysts. Figure 3.5 represents the schematic diagram of SEM. A Hitachi S900 SEM unit operating at 10 KeV will be used; it is capable of imaging at very high resolutions, of up to 0.5 nm. SEM samples will be prepared by spreading catalyst on the surface of specimen, and then chromium is coated to enhance the conductivity of the sample. In the SEM machine, an electron gun is used to generate an electron beam with high intensity. When the beam bombards the metal-coated specimen, secondary and backscattered electrons are emitted from the highlighted area. Thereafter, the electrons are captured by specific detectors and the resulting image further processed. The contrast of the image is due to the difference in the electron collection efficiency, which is affected by the angle of emission, surface relief, and atomic number of elements (Bergeret & Gallezot, 1997). FESEM is an acronym for Field Emission Scanning Electron Microscope. It is a microscope that uses electron scanned beam in raster mode (Khanlou, 2012). FESEM is an upgrade version of SEM; it leads to a clearer three-dimensional image for the surface of the samples (Suzuki, 2002; Brabazon & Raffer, 2010). In particular, FESEM has also been mounted with Energy Dispersive X-ray (EDX) which for the X-ray excitation of samples to identify the composition of various structural phases (Kandaswamy *et al.*, 2012). Besides that, the X-ray excitation of samples is able to characterize the peaks of X-ray spectrum based on the atomic structure too (Lausmaa *et al.*, 1990).

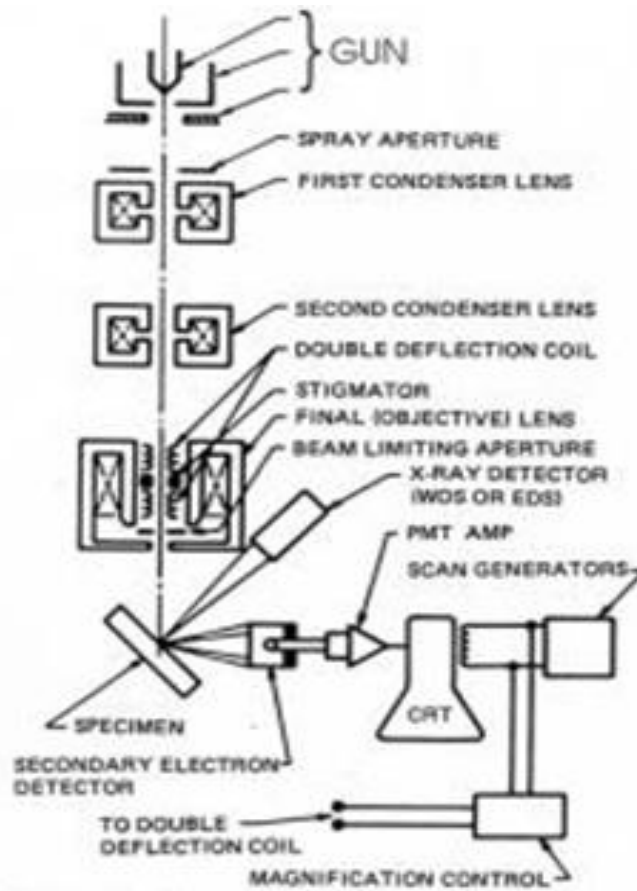


Figure 3.5: Schematic diagram of SEM

3.4.4 Thermogravimetric Analysis

Thermogravimetric analysis or TGA is the equipment that is employed to determine weight changes of sample as a function of time or temperature under a controlled atmosphere (Wieboldt *et al.*, 1988; Demessie *et al.*, 2011). Significantly, TGA is also often used to carry out quantitative analysis for kinetics and mechanism studies of sample-gas interaction (Tzeng *et al.*, 2010). Typical TGA is capable of running an analysis from 25 to 900 °C with the maximum limitation of 1000 °C. The weight of the sample should be in the range of 1-150 mg with sample weighing more than 25 mg is preferable for higher accuracy (Anderson, 2012). Figure 3.7 shows a typical TGA profile that be obtained. It depicts a weight loss over a few different stages (temperature).

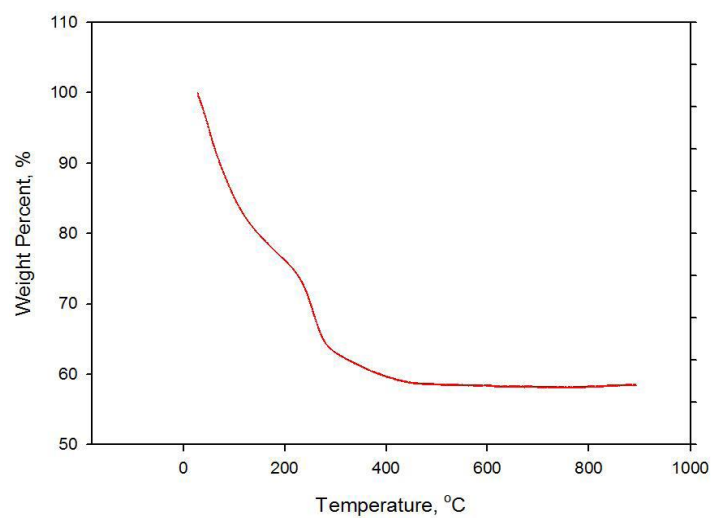


Figure 3.6: Weight Percent Loss against Temperature from TGA

In this research, Q500 TGA unit is employed for all solid sample-gases interaction studies as shown in Figure 3.8.



Figure 3.7: Thermogravimetric Analysis Q500

3.5 Reactor Setup

It is desired to study the glycerol dry reforming reaction in a fixed bed reactor at 1 atm and reaction temperatures of 650 to 750°C. The catalytic evaluation is carried out by placing 0.20 g of catalyst into the quartz glass fixed-bed reactor (ID: 10 mm) supported by two layers of quartz wool. CO₂ and glycerol will be metered into the reactor using digital flow controller. The reaction is carried out for 2 h and held at 700 °C. After that, the composition of syngas produced was determined by online Agilent 3000 micro-gas chromatography (GC) with TCD column, Backflush Molecular Sieve 5A and Plot U column.

3.6 Glycerol Reforming

Reaction runs will be conducted on a computer-controlled experimental rig consisting of a gas manifold station, a glass tube fixed-bed reactor (OD = 6.25 mm and ID = 4.57 mm) packed with 0.2 g of catalyst, and a Shimadzu GC-17A gas chromatograph fitted with a thermal conductivity detector and an Alltech CTR-1 column. Prior to each reaction, the calcined catalyst was reduced in situ in 50 mL min⁻¹ of 50% H₂/N₂ mixture at temperature ramp of 5 °C min⁻¹, and held at 790 °C for 2 h. Following activation of the catalyst, the reactor will be cooled under a blanket of N₂ to the reaction temperature. Gas-hourly space velocity of 20,000 h⁻¹ and catalyst particles limited to the size range 140–250µm to minimize transport-disguised kinetics during data analysis. All the runs will be conducted over the temperature range 650–750 °C with constant total pressure of 110 kPa. The N₂ will be employed as the diluent gas and tie component for material balance purposes. Figure 3.8 below shows the similar design of the glycerol reforming system.

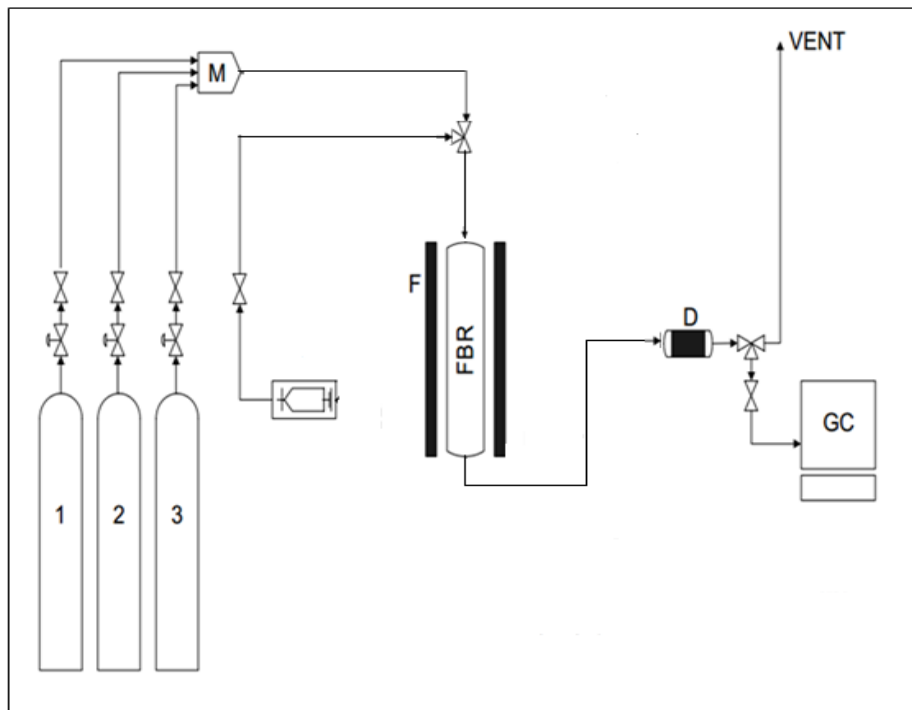


Figure 3.8: Glycerol Reforming System

Note:

1: Carbon Dioxide

2: Nitrogen

3: Hydrogen

M: Mixer

H: HPLC Pump

F: Electrical Furnace

FBR: Fixed-bed Reactor

D: Drierite Bed

GC: Micro Gas Chromatography

3.7 Fixed-Bed Reactor

The cross sectional image of the injector fixed-bed reactor system is shown in the Figure 3.9. This particular reactor system is the ‘hub’ within the whole reactor setting. The similar design of fixed-bed reactor was used in this research. The injector of the reactor

was used to introduce the glycerol solution into the fixed-bed reactor and make sure that the flow of the liquid column flow continuously under heating condition by the electrical furnace. The injector was made of 5/16" stainless steel tube which compacted with quartz wool. The tubular reactor was designed by 1/2" glass tube with an inner diameter of 10mm. Then, the catalyst bed supporter within the reactor was made of quartz wool which was located in the middle of the glass tube which was also estimated to be the center point of the electrical furnace. This was to ensure that the heat could be uniformly distributed within the catalyst bed. After that, the 1/16" K-type thermocouple was ensured to be able to reach and touch the catalyst bed in order to gain the actual temperature of the catalyst bed accurately.

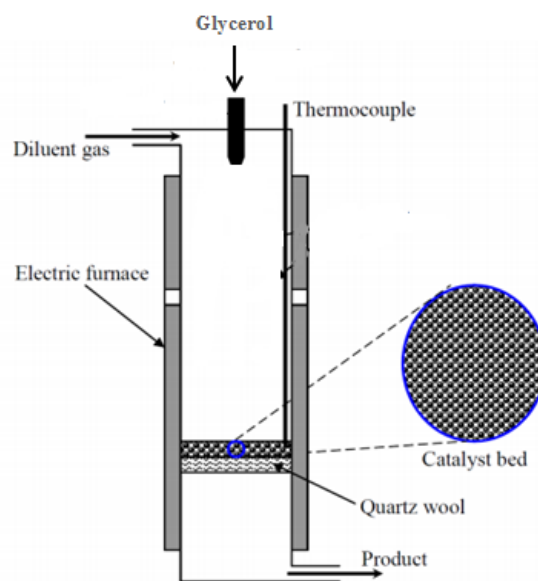


Figure 3.9: Schematic diagram of the Tubular Reactor for Glycerol Reforming

CHAPTER 4

RESULTS AND DISCUSSION

4.1 Introduction

One of the current research scopes is to determine catalyst physiochemical properties and further justifying their catalytic performance. Therefore, the catalysts prepared were analysed before the reaction of glycerol is performed. The techniques employed to characterize the catalysts include BET, XRD, XPS, FESEM-EDX and TGA. The results obtained from some techniques are discussed in this section.

4.2 Characterization of the fresh catalyst

4.2.1 Liquid N₂ Physisorption by Brunauer Emmett Teller (BET)

The textural properties of the fresh Ce-Ni/MgO catalysts were characterized using liquid N₂ physisorption technique. Figures 4.1 and Figure 4.2 show the isotherm plot of Ce-Ni/MgO catalysts with 3 wt% and 5 wt% cerium loadings respectively. The hysteresis pattern has conclusively shown that the catalysts are mesoporous materials.

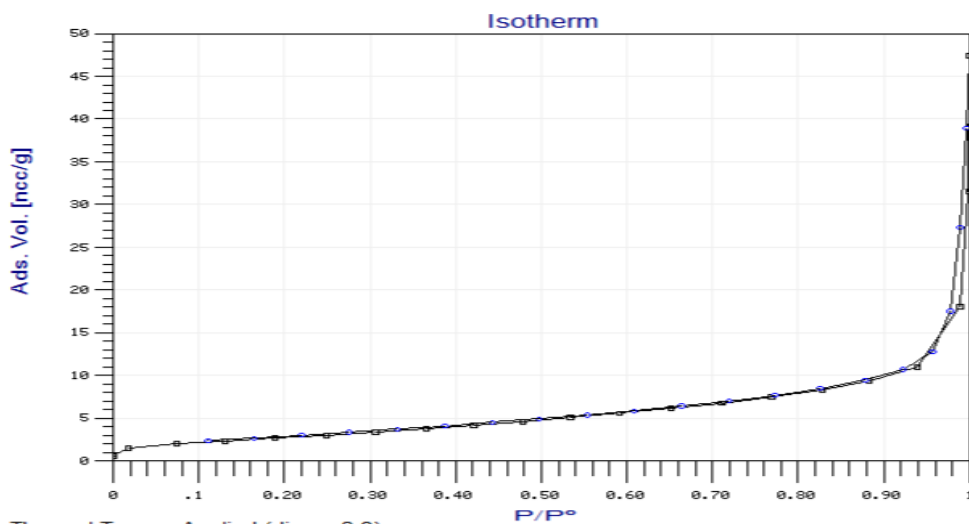


Figure 4.1: Isotherm plot for 3 wt% cerium-promoted Ni/MgO

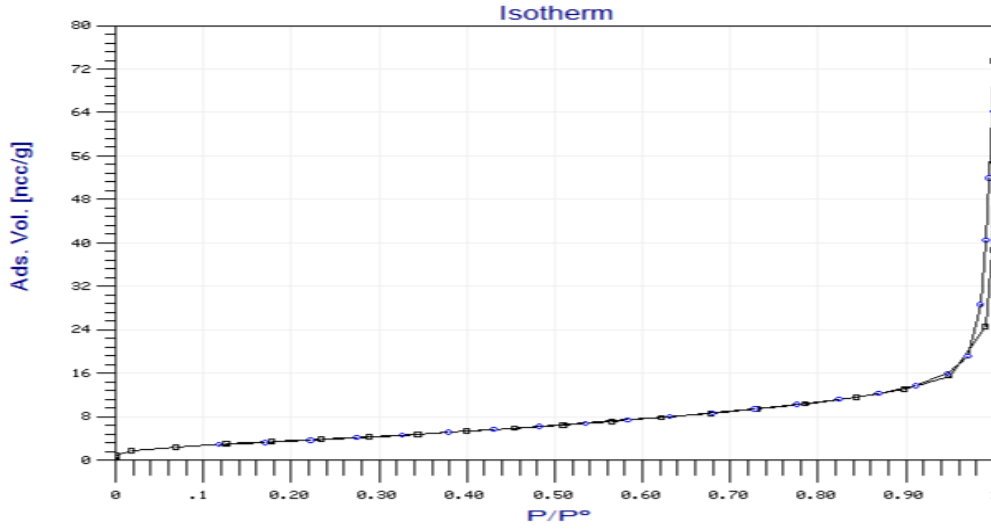


Figure 4.2: Isotherm plot for 5 wt% cerium-promoted Ni/MgO

Table 4.1: BET specific surface area, pore volume and pore diameter of the catalyst samples

Samples of catalysts (wt% Ce)	BET specific surface area (m^2g^{-1})	Pore volume (cm^3g^{-1})	Pore diameter (nm)
3	10.59	0.0035	0.88
5	14.00	0.0045	0.96

Table 4.1 shows that 5 wt% Ce-Ni/MgO catalysts have only slightly larger BET specific surface area than 3 wt% Ce-Ni/MgO with the same pore volume. The pore volume of 3 wt% Ce-Ni/MgO catalyst is slightly larger than that of 5 wt% Ce-Ni/MgO catalyst. It may be due to the pore blockage of MgO support by cerium oxide particles (Adriana et al., 2012). However, the pore diameter of 3 wt% Ce-Ni/MgO catalyst is slightly smaller

than that of 5 wt% Ce-Ni/MgO catalyst. It also shows that the nickel metal is well dispersed on the MgO support even with the increased loadings of cerium.

4.2.2 FESEM-EDX Imaging

The topography and morphology of fresh catalyst was further studied by FESEM. Figure 4.3 show that the 5 wt% cerium-promoted Ni/MgO catalyst is a crystalline catalyst.

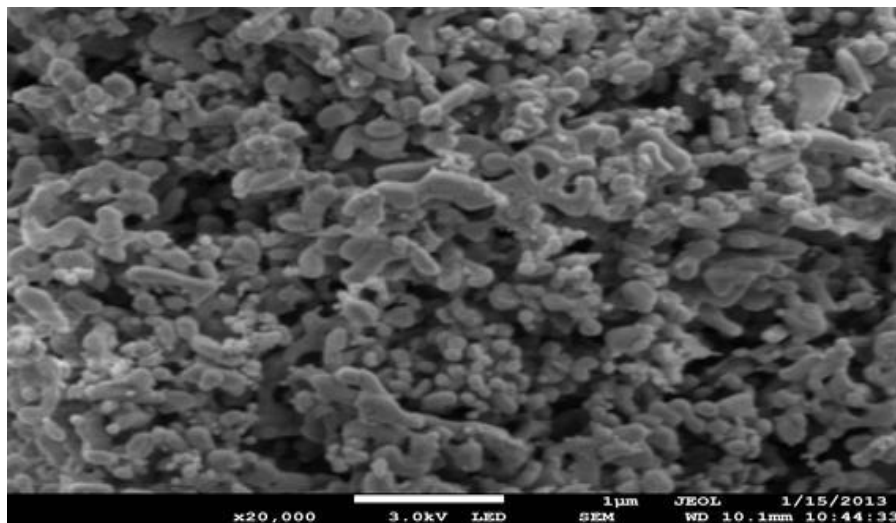


Figure 4.3: SEM image of 5 wt% Ce-promoted Ni/MgO catalyst

Figure 4.4 depicts the quantification of the atomic elements contained in the 5 wt% Ce-promoted Ni/MgO catalyst in terms of atomic percentage concentration. Through the EDX intensity graphs, different elements can be identified by observing their intensity because which will lead to different peak. For example, the elements such as nickel and cerium are detected with their corresponding weight percentages are 23.49 wt% and 3.46 wt% respectively. The concentrations of the elements Mg and O are attributed to the MgO support of the catalyst. The existence of carbon in the result is acceptable because of the carbon tape that is used to stick the samples on the holder to be analysed by FESEM-EDX. A small quantity of carbon is found for the catalyst, which contributes to the weight percentage of 2.81 wt% to the catalyst. It proves that addition of cerium as promoter can reduce the carbon deposition on the catalyst effectively. This is because the

cerium has high oxygen storage capability therefore carbon deposited on the catalyst will tend to react with oxygen to form carbon dioxide thus enhancing the cleaning ability of carbon from the catalyst surface (Daza et al., 2010).

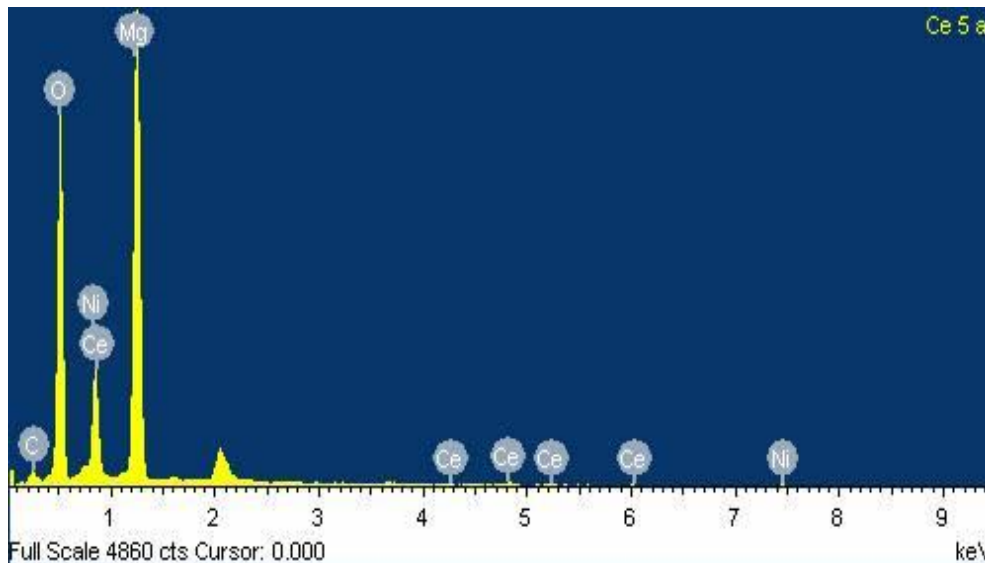


Figure 4.4: EDX graph of 5 wt% Ce-promoted Ni/MgO catalyst

4.2.3 X-Ray Diffraction (XRD)

The crystalline phase of 5 wt%-Ce-promoted Ni/MgO was identified by using XRD techniques. XRD is a non-destructive analytical technique which is widely used to identify the crystalline structure, crystalline phase and also the size of crystallites of natural or synthetic materials. Table 4.2 shows the summary of values of 2θ , intensity and inter plane distance of crystal (d-spacing) together with crystallite size for the diffraction peaks. Besides, from Figure 4.5, XRD patterns show the effect of Ce addition to the catalyst as the peaks appeared at $2\theta = 28.53^\circ$ and 47.46° . At $2\theta = 33.05^\circ$, 42.99° , 59.06° and 62.41° , the peaks formed represents the formation of the NiO-MgO solid solution. The NiO-MgO solid solution is known to be extremely difficult to reduce and thus exhibits high intensity especially at $2\theta = 42.99^\circ$. The formation of a NiO-MgO solid solution after catalyst calcination is consistent with what has been reported by

previous studies (Djaidja et al., 2006). MgO has the same crystal structure as NiO and they combine to form a predominantly basic solution (Hu et al., 1999). The surface of the solid solution favors the adsorption of CO₂ and the small particle size of nickel, thus inhibiting the carbon deposition (Ruckenstein et al, 1995). At around $2\theta = 42.99^\circ$, the peak has sharp intensity indicating that the catalyst has good crystallinity as shown in Figure 4.5 with the absent amorphous phase.

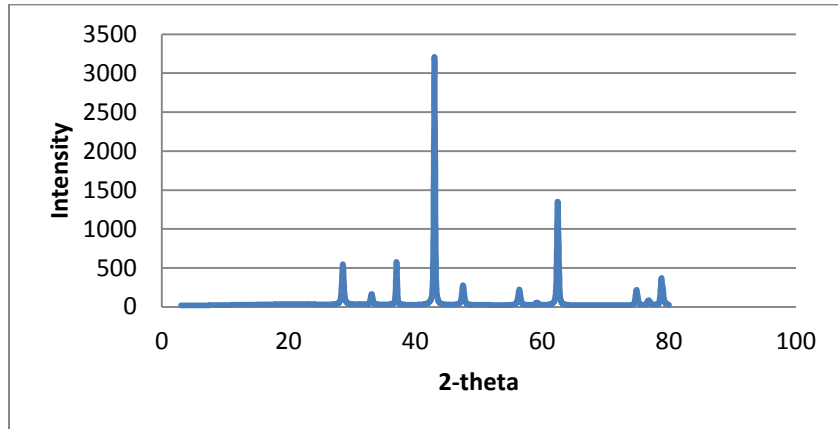


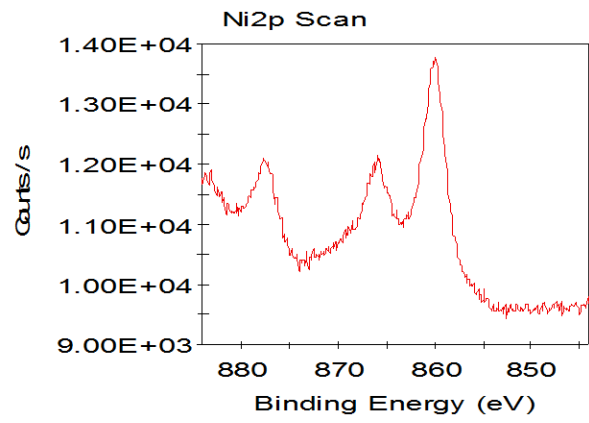
Figure 4.5: XRD patterns for 5 wt% Ce-promoted Ni/MgO catalyst

Table 4.2: Summary of values of 2-theta, intensity, inter plane distance of crystal (d-spacing) and crystallite size for the diffraction peaks

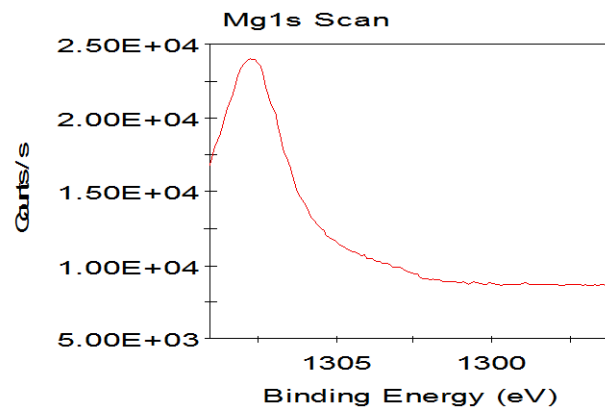
2-theta (degree)	Intensity	d (ang)	Crystallite size
28.53(10)	551.27887	3.1259(10)	242(5)
33.05(19)	166.017188	2.7079(15)	236(10)
37.00(9)	577.636884	2.427(6)	429(17)
42.99(5)	3209.358259	2.1023(2)	417(8)
47.46(16)	278.663502	1.9142(6)	243(8)
56.36(2)	225.01115	47.457(16)	256(15)
59.06(7)	55.178806	56.36(2)	186(18)
62.41(5)	1352.434934	1.48681(11)	398(9)
74.84(14)	219.140402	1.2677(2)	331(16)
76.76(4)	85.191902	1.2407(6)	241(19)
78.79(7)	373.862964	1.21373(9)	370(11)

4.2.4 X-ray Photoelectron Spectroscopy (XPS)

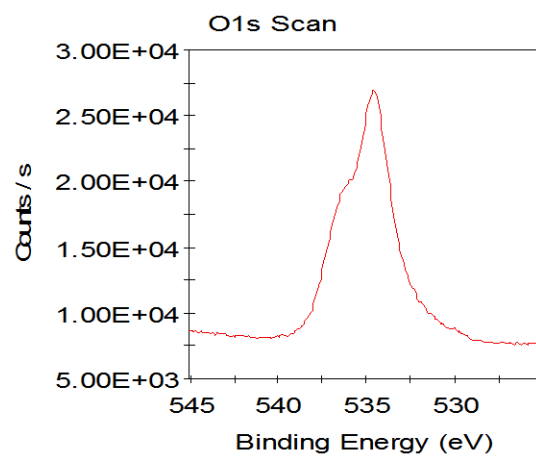
Figure 4.6 shows XP spectra of Ni2p, Mg1s and O1s of fresh Ni/MgO catalyst while the Table 4.3 summarized the binding energy of each element in the catalyst and their corresponding counts per unit second. Ni2p can be deconvoluted in three components centered at 859.98, 868.88 and 877.68 eV. The three components can be assigned with Ni⁰ and Ni²⁺ probably as NiO or Ni(OH)₂ due to the asymmetry of the signals. The main signal at 1307.78 eV corresponds to Mg1s associated with MgO. The signal at 534.58 eV refers to the existence of O1s element in the catalyst. It is associated with the formation of NiO and MgO.



(a)



(b)



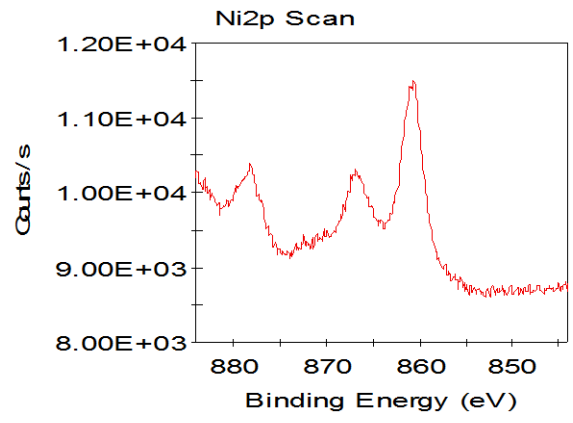
(c)

Figure 4.6: XP spectra of (a) Ni2p (b) Mg1s (c) O1s of fresh Ni/MgO catalyst

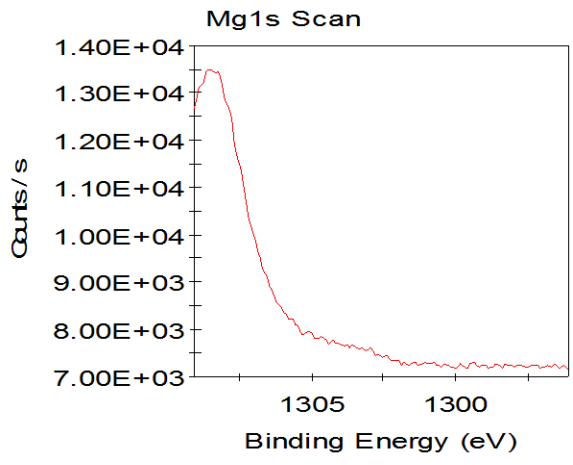
Table 4.3: Binding energies of each element in fresh Ni/MgO catalyst and their corresponding count per unit second

Elements		Binding energy (eV)	Counts /s
Ni2p	Start	844.08	9685.64
	Peak	859.98	13719.6
	End	884.08	11755
Mg1s	Start	1296.08	8603.51
	Peak	1307.78	24066.9
	End	1309.08	16717.4
O1s	Start	525.08	7633.5
	Peak	534.58	26924.5
	End	540.08	8599.98

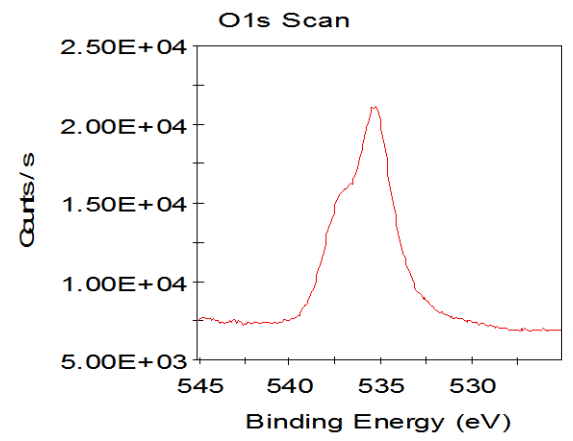
Figure 4.7 shows XP spectra of Ni2p, Mg1s, O1s and Ce3d of fresh 3wt% Ce-Ni/MgO catalyst while Table 4.4 summarized the binding energies of each element in the catalyst and their corresponding counts per unit second. For this catalyst, the three components deconvoluted at 860.58, 866.88 and 878.18 eV correspond to Ni⁰ and Ni²⁺ probably as NiO or Ni(OH)₂ due to the asymmetry of the signals. The presence of Mg1s at 1308.48 eV is associated with MgO. The main signal at 535.48 eV refers to O1s which is the element of NiO or MgO in the catalyst. The deconvolution of Ce3d at 878.08, 887.18, 903.98 and 921.88 eV can be associated with the presence of Ce³⁺ and Ce⁴⁺. However, Ce is mostly found as Ce⁴⁺ in mixed oxide.



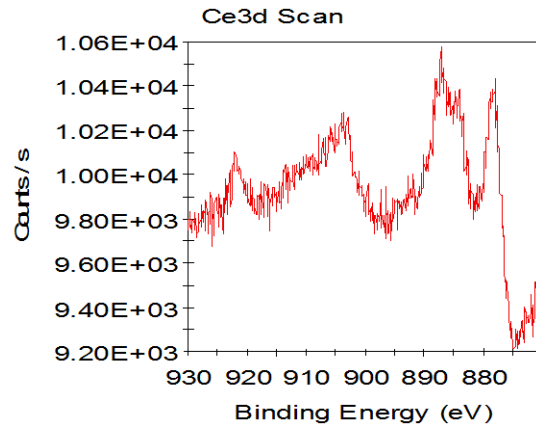
(a)



(b)



(c)



(d)

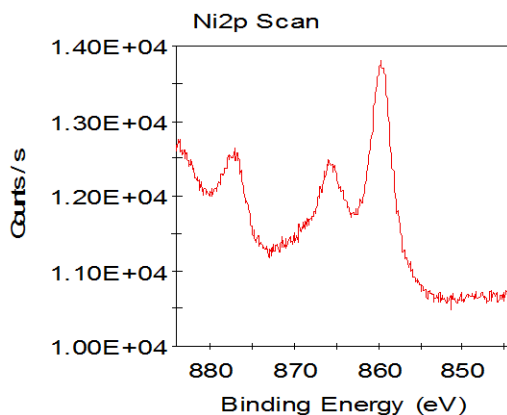
Figure 4.7: XP spectra of (a) Ni2p (b) Mg1s (c) O1s (d) Ce3d of fresh 3wt% CeNi/MgO catalyst

Table 4.4: Binding energies of each element in fresh 3wt% Ce-Ni/MgO catalyst and their corresponding counts per unit second

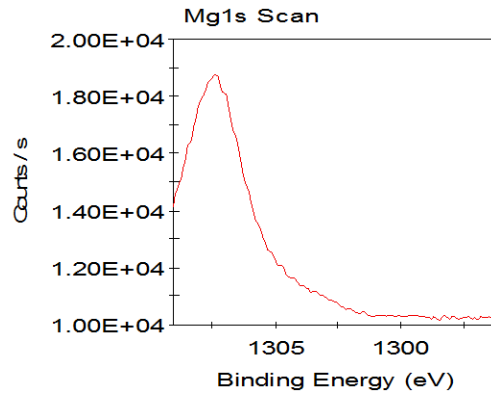
Elements		Binding energy (eV)	Counts /s
Ni2p	Start	844.08	8793.54
	Peak	860.58	11496.5
	End	884.08	10199
Mg1s	Start	1296.08	7150.09
	Peak	1308.48	13499.1
	End	1309.08	12690.6

O1s	Start	525.08	6943.08
	Peak	535.48	21134.1
	End	545.08	7536.16
Ce3d	Start	870.08	9470.93
	Peak	887.18	10578.4
	End	930.08	9750.46

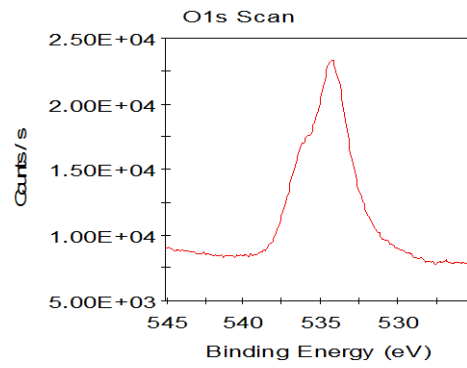
Figure 4.8 shows XP spectra of Ni2p, Mg1s, O1s and Ce3d of fresh 5wt% Ce-Ni/MgO catalyst. Table 4.5 lists the binding energies of each element in the catalyst and their corresponding counts per unit second. Ni2p is deconvoluted into three components located at 859.68, 866.08 and 877.08 eV. The three components are associated with Ni⁰ and Ni²⁺ probably as NiO or Ni(OH)₂ due to the asymmetry of the signals. The binding energy of 1307.38 eV in Mg1s spectrum corresponds to Mg²⁺ in MgO support. O1s element at 535.48 eV relates to O²⁻ found in the formation of NiO or MgO. In Ce3d spectrum, main signals are observed at 876.98, 885.78, 902.98 and 920.78 eV. The main signals can be explained by the presence of Ce³⁺ and Ce⁴⁺ in the catalyst. However, the amount of Ce⁴⁺ is larger than that of Ce³⁺ in the catalyst.



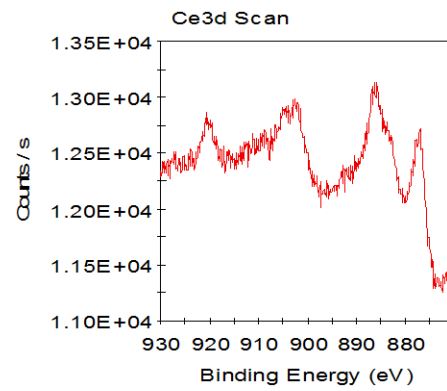
(a)



(b)



(c)



(d)

Figure 4.8: XP spectra of (a) Ni2p (b) Mg1s (c) O1s (d) Ce3d of fresh 5wt% Ce-Ni/MgO catalyst

Table 4.5: Binding energies of each element in fresh 5wt% Ce-Ni/MgO catalyst and their corresponding counts per unit second

Elements		Binding energy (eV)	Counts /s
Ni2p	Start	844.08	10712.1
	Peak	859.68	13797.1
	End	884.08	12676.6
Mg1s	Start	1296.08	10200
	Peak	1307.38	18742.9
	End	1309.08	14134.6
O1s	Start	525.08	7808.28
	Peak	534.28	23349.3
	End	545.08	9005.32
Ce3d	Start	870.08	11493.3
	Peak	885.78	13139.1
	End	930.08	12347.7

4.2.5 Thermo Gravimetric Analysis (TGA)

From the TGA result obtained for each catalyst, the existence of small peaks at the temperatures below 200°C was due to the water elimination from the catalyst whereas the peak hovered in between 330°C and 360°C was attributed to the Ni(NO₃)₂ decomposition into NiO. For each heating ramp, there are slight changes of the maximum peak when 5% Ce are promoted to Ni/MgO catalysts. Figures 4.9 and 4.10 depict the graphs of derivative weight versus peak temperature for dry Ni/MgO catalyst and 5% Ce-Ni/MgO catalyst respectively at the heating ramp of 10°C/min. For the heating ramp of 10°C/min, 5% Ce-Ni/MgO catalyst gives a slightly higher peak compared to Ni/MgO catalyst. This

implies that the extent of decomposition of $\text{Ni}(\text{NO}_3)_2$ into NiO is higher with the existence of Ce as promoter to the catalyst.

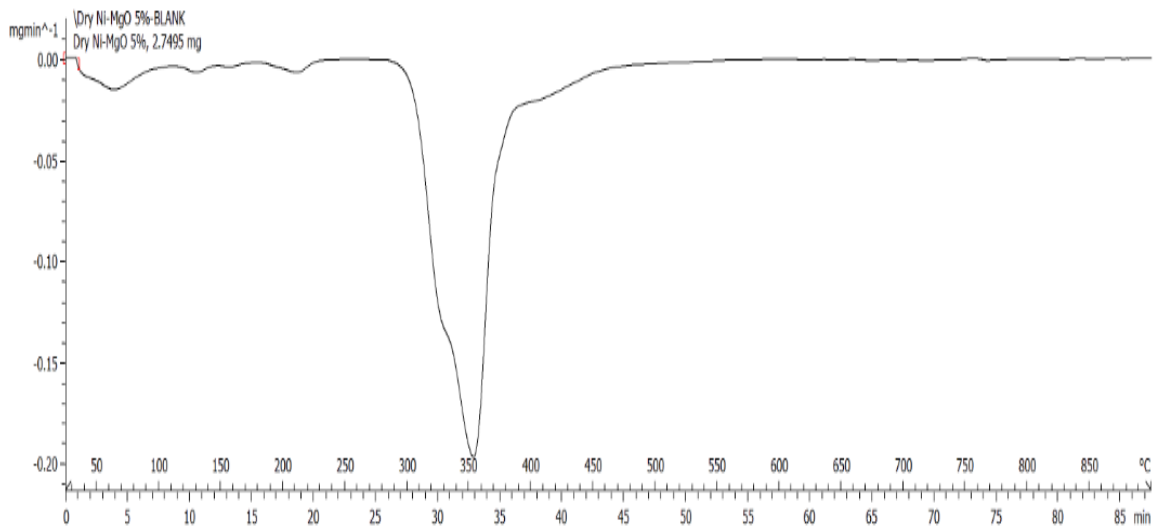


Figure 4.9: Graph of derivative weight versus peak temperature for Ni/MgO catalyst at the heating ramp of 10°C/min

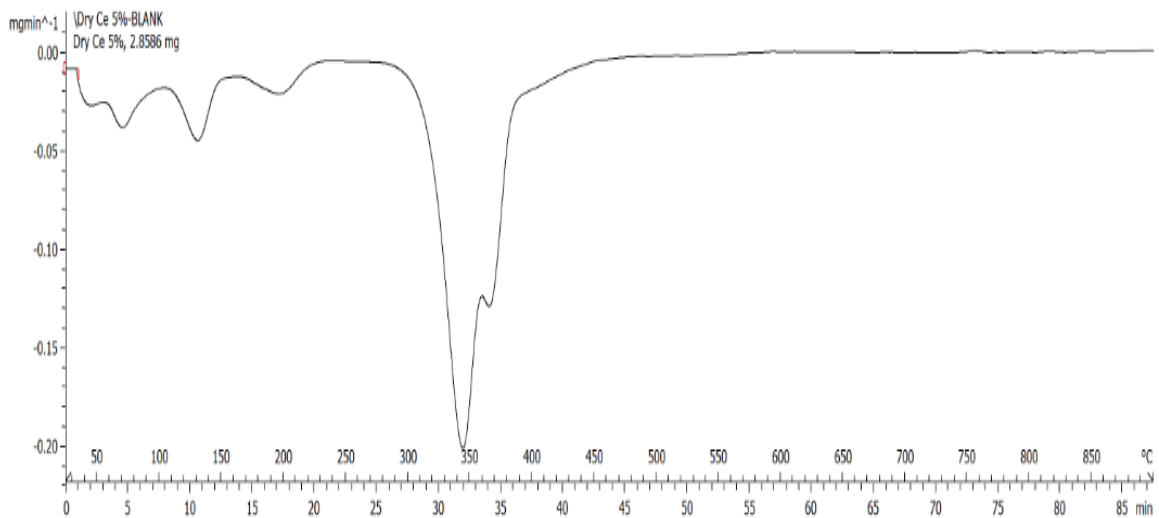


Figure 4.10: Graph of derivative weight versus peak temperature for 5wt% Ce-Ni/MgO catalyst for the heating ramp of 10°C/min

Besides, three different heating ramps viz. 10°C/min, 15 °C/min and 20 °C/min were used for temperature-programmed calcinations studies to investigate the gas-solid interaction during the calcinations and to determine the calcination temperatures for the catalysts that were subsequently employed in the reaction. Moreover, the graphs of derivative weight versus peak temperature for 5 wt% Ce-Ni/MgO catalyst at the heating ramps of 15 °C/min and 20 °C/min are shown by Figures 4.11 and 4.12 respectively. It can be observed that when the heating ramp increases, the magnitude of the highest peak becomes higher. Besides, the highest peak has also shifted to the higher temperature range as the heating rate increases. This trend was tolerable with the Kissinger proposition and thus can be adequately represented by the model-free Kissinger equation.

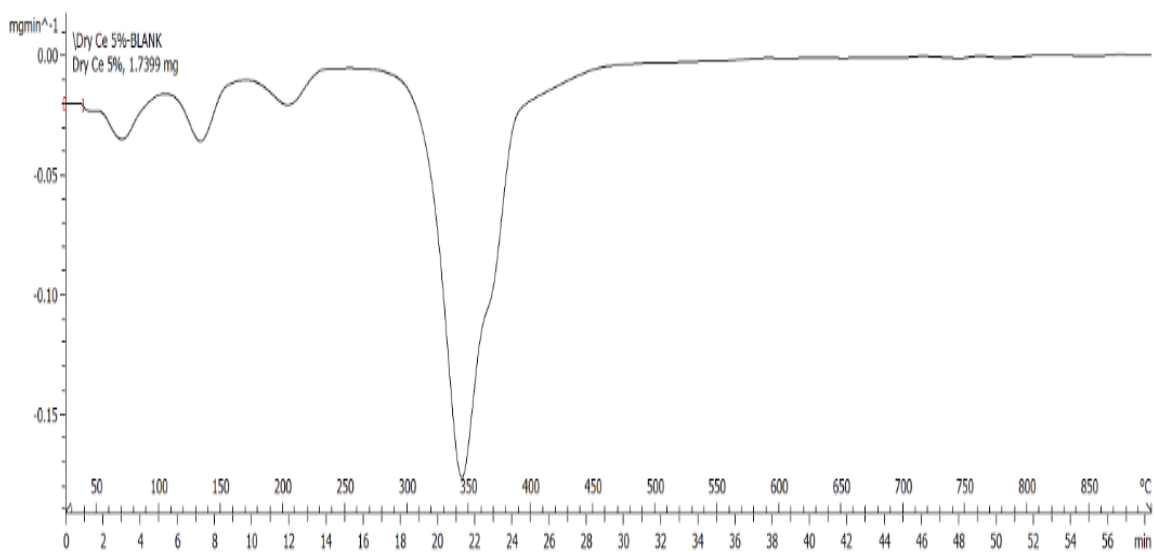


Figure 4.11: Graph of derivative weight versus peak temperature for 5wt% Ce-Ni/MgO catalyst for the heating ramp of 15°C/min

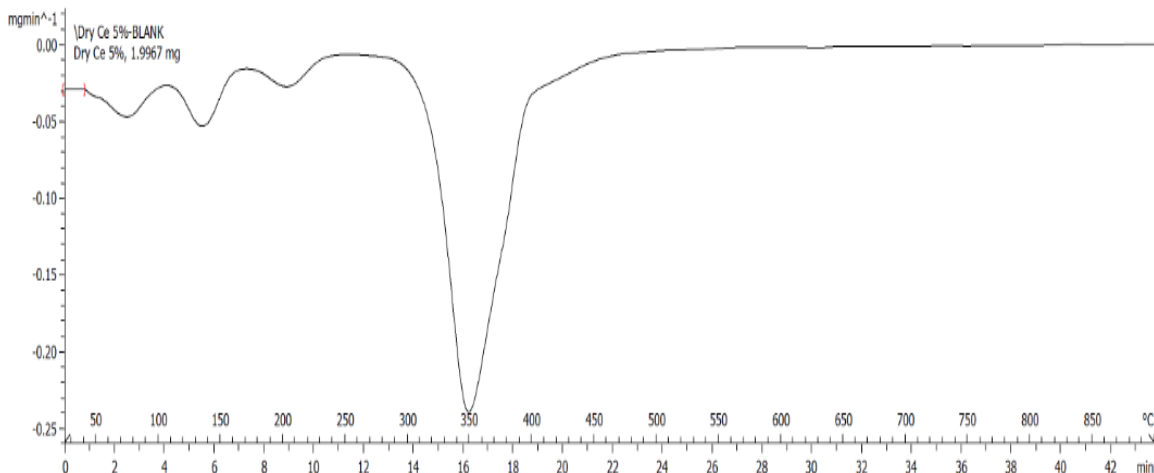


Figure 4.12: Graph of derivative weight versus peak temperature for 5wt% Ce-Ni/MgO catalyst for the heating ramp of 20°C/min

Table 4.6: Results of the maximum peak temperature for two non-calcined catalyst samples at three different heating ramps.

Sample (wt% Ce)	Heating ramps (°C/min)		
	10	15	20
0	355	360	365
5	345	348	350

Table 4.6 depicts the results of the maximum peak temperature for two non-calcined catalyst samples at three different heating ramps. The activation energy values associated with calcination procedures of all catalyst samples were subsequently determined by using Kissinger model. Kissinger model proposes that a plot of $\ln(\frac{\beta}{T_p^2})$ versus $\frac{1}{T_p}$ will produce a straight line from which the activation energy of the catalyst can be determined where by β and T_p represent the heating ramp and maximum peak temperature respectively. Figure 4.12 shows the plot of Kissinger model for the two different catalysts.

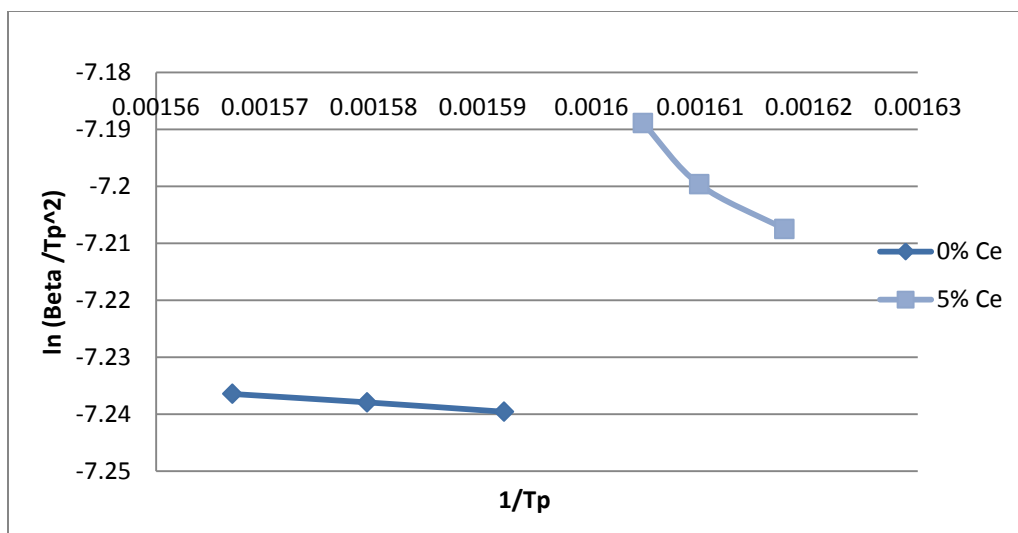


Figure 4.13: Plot of Kissinger model for two different catalysts

Table 4.7 summarized the activation energy, E_a of Ni/MgO and 5%-Ce-Ni/MgO catalysts during calcination. From the results, it was obvious that 5% Ce-Ni/MgO catalyst contain far higher activation energy than Ni/MgO catalyst. Besides, it also showed that Ce-Ni/MgO is highly stable due to the stronger metal-metal interaction which is ionic bond in the catalyst.

Table 4.7: Activation energy of catalyst samples

Sample (wt% Ce)	E_a (J/mol)	Accuracy, R^2
0	1038.93	0.9992
5	11904.83	0.9571

4.3 Glycerol reforming reaction studies

4.3.1 The conversion of main reactant (glycerol)

The 3 wt% of calcined Ce-Ni/MgO catalyst was used to determine the conversion of the main reactant (glycerol) at fixed temperature by the reforming process. The results were taken first and second hours after the reaction started. From the results, the glycerol conversion, X_G was directly proportional with the reactant (glycerol to N_2) flow ratios. Besides, it can be observed that the glycerol conversion at both temperatures for the first hour is higher than second hour indicating the conversion decreases as the reaction going further. Figure 4.13 depicts the increasing trend of X_G as the reactant flow ratios increased at 700 °C for the first and second hours whereas the plot of glycerol conversion, X_G at 750 °C is shown by Figure 4.14.

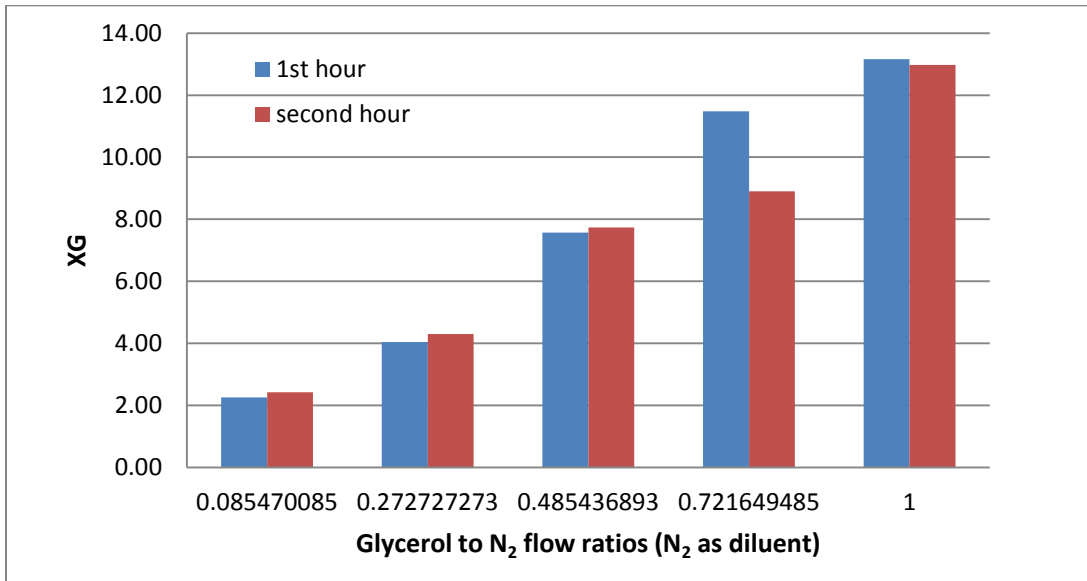


Figure 4.14: Plot of glycerol conversion, X_G vs flow ratios at (700 °C, 1 atm) for the first and second hours

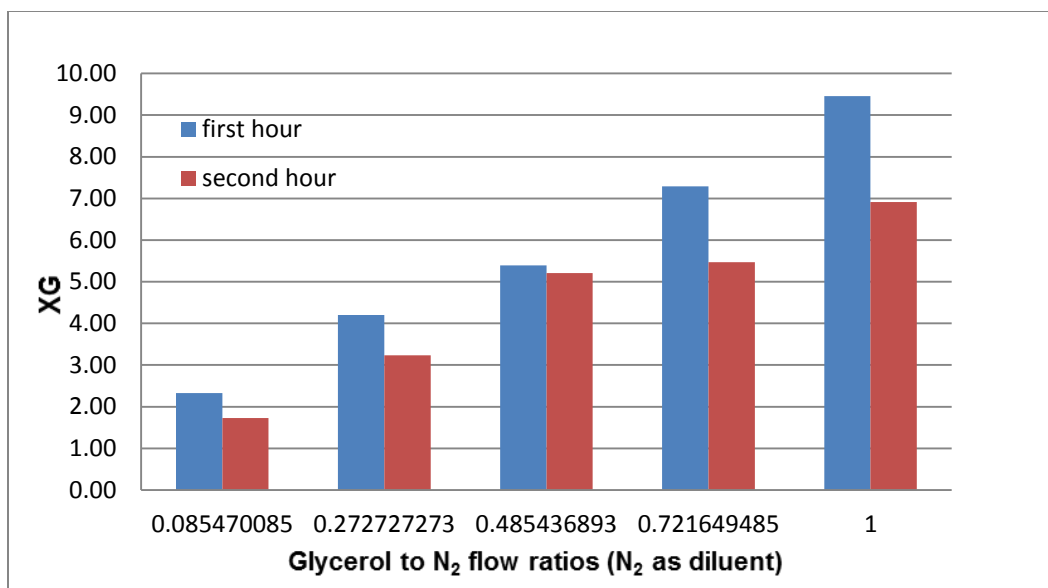


Figure 4.15: Plot of glycerol conversion, X_G vs flow ratios at (750 °C, 1 atm) for the first and second hours

4.3.2 Effect of Reaction Temperature

Reaction studies have found that 3 wt% Ce-Ni/MgO catalysts attributed almost equal rate of formation of product yield (H_2 and CO). Besides, the ratio of H_2 to CO for 3 wt% catalysts is greater than unity. Therefore, it can be said that the promoter Ce not only has improved the reactivity of catalyst, but also provides an alternative pathway that can boost up the H_2 : CO ratio, most likely the enhancement of glycerol cracking for higher H_2 production rate. The catalyst was employed for further studies regarding the influence of reaction temperature on the reaction rates with Glycerol to N_2 flow ratios = 1. Based on the Arrhenius principle, the reforming temperature would affect the reaction rate as indicated by the Arrhenius equation $k = A(\exp -\frac{E}{RT})$ where k = rate constant. Graphs of rate of formations, $\ln(r_i)$ versus $\frac{1}{T}$ of different reaction rates were plotted for the first and second hours which are shown in Figure 4.15 and Figure 4.16 respectively. The i symbol indicates the various components such as H_2 , CH_4 , CO_2 and CO.

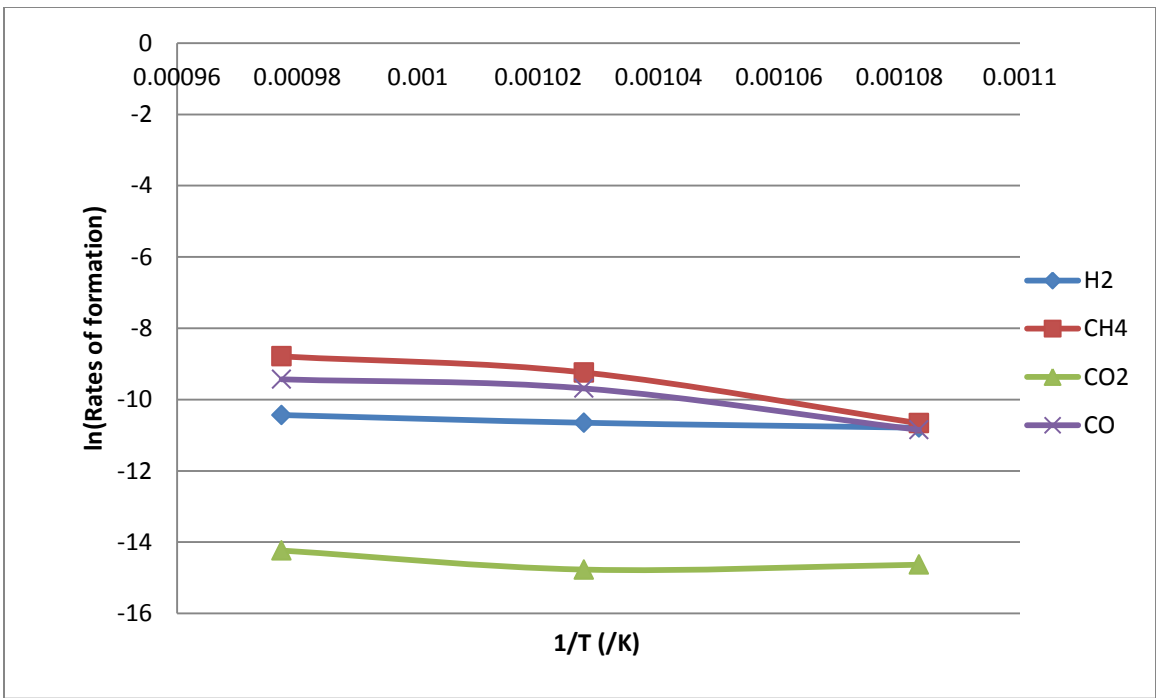


Figure 4.16: Plot of various rates of formation of each component for the first hour of the reaction

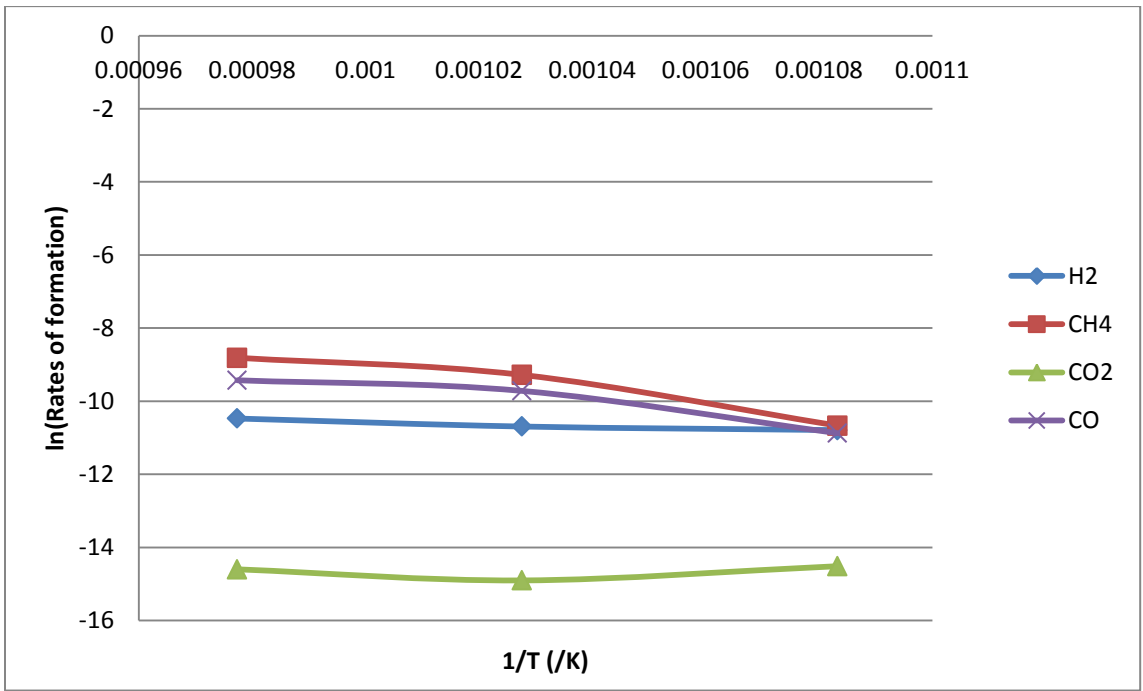


Figure 4.17: Plot of various rates of formation of each component for the second hour of the reaction

From the slope of best fit, the activation energy for H₂ was determined and compared between the first and second hours of the reaction. The activation energy, E_a obtained for H₂ formation rate at the first hour was 27.82 kJ/mol and at the second hour was 24.71 kJ/mol. The fairly low E_a for both intervals indicated that the catalyst was very active in promoting the hydrogen production from the glycerol. Besides, it is obvious that the E_a at the second hour is lower which implies that the catalyst become more active in the reaction as time passing by.

CHAPTER 5

CONCLUSIONS AND RECOMMENDATIONS

5.1 Conclusions

From the BET characterization, it can be concluded that the 5 wt% Ce-Ni/MgO catalyst has larger BET specific surface area indicating that the nickel metal is well dispersed on the MgO support even with the increased Ce loadings. In addition, the pore volume and pore diameter of 5 wt% Ce-Ni/MgO catalyst are slightly larger than that of 3 wt% Ce-Ni/MgO catalyst. The topography of the catalyst is observed from the FESEM imaging. It can be observed that the metallic particles in 5 wt% Ce-Ni/MgO catalyst are uniformly distributed. Furthermore, the result of EDX for the fresh 5 wt% Ce-Ni/MgO catalyst shows that only small amount of carbon is found for the catalyst which proving that the carbon removal efficiency of the catalyst is high. Besides, XRD diffraction patterns of fresh 5wt% Ce-Ni/MgO catalyst showed peaks representing MgO at $2\theta = 37.00^\circ$ and NiO at 42.99° , 62.41° , 74.84° and 78.79° . The peak at 42.99° has sharp intensity indicating that the catalyst has good crystallinity and amorphous phase is not present.

Moreover, the catalysts were also further characterized by XPS. XP spectra of fresh Ni/MgO catalyst showed the deconvolution of Ni2p in three components at 859.98, 868.88 and 877.68 eV, existence of Mg1s at 1307.78 eV and O1s at 534.58 eV. While, XP spectra of fresh 3 wt% Ce-Ni/MgO catalyst showed deconvolution of Ni2p in three components at 860.58, 866.88 and 878.18 eV, there is the existence of Mg1s at 1308.48 eV and O1s at 535.48 eV. Other than that, for fresh 3 wt% Ce-Ni/MgO catalyst, Ce3d is found to be deconvoluted at 878.08, 887.18, 903.98 and 921.88 eV. XP spectra of fresh 5 wt% Ce-Ni/MgO catalyst showed the deconvolution of Ni2p in three components at 859.68, 866.08 and 877.08 eV, presence of Mg1s are at 1307.38 eV and O1s at 535.48 eV. In addition, main signals of Ce3d are observed at 876.98, 885.78, 902.8 and 920.78 eV. Meanwhile, from the TGA results of Ni/MgO and 5 wt% Ce-Ni/MgO catalysts, the

heating ramp of 10°C/min, 5 wt% Ce-Ni/MgO catalyst gives a slightly higher peak compared to Ni/MgO catalyst implies that promotion of Ce to the catalyst gives a greater extent of decomposition of Ni(NO₃)₂ into NiO. For the Kissinger model of the two catalysts, it was obvious that 5 wt% Ce-Ni/MgO catalysts contain much higher activation energy than Ni/MgO catalyst indicating that the catalyst is highly stable due to the stronger metal-metal interactions in the catalyst.

The reaction studies summarized that the glycerol conversion, X_G was directly proportional with the reactant (glycerol to N₂) flow ratios. The glycerol conversion at 700 °C and 750 °C for the first hour is higher than second hour indicating the conversion decreases as the reaction going further. Besides, the ratio of H₂ to CO for 3 wt% catalysts is greater than unity. Therefore, it can be said that the promoter Ce not only has improved the reactivity of catalyst, but also provides an alternative pathway that can boost up the H₂: CO ratio, most likely the enhancement of glycerol cracking for higher H₂ production rate. The catalyst was employed for further studies regarding the influence of reaction temperature. The increasing temperature results in increase of the rates of formation of both CO and H₂ gas and this is in accordance to the Arrhenius principle which proposed that the rate of reaction is directly proportional to the reaction temperature. From the slope of best fit, the activation energy, E_a obtained for H₂ formation rate at the first hour was 27.82 kJ/mol and at the second hour was 24.71 kJ/mol. The fairly low E_a for both intervals indicated that the catalyst was very active in promoting the hydrogen production from the glycerol. Besides, it is obvious that the E_a at the second hour is lower which implies that the catalyst become more active as the reaction going.

5.2 Recommendations

1. Based on the findings and observation of this research project, the following suggestions are proposed for future studies:
2. The effect of pressure of feed mixture on the composition of product yield can be investigated. Varying feed pressure seems to be interesting to study the influence on the composition of product yield.

3. The catalyst should be gasified by H_2/N_2 gas held at 2h in order to activate the catalyst before the reaction started. Products yield may probably increase.
4. Different types of promoters will also influence the catalyst performance. La promoted catalyst is recommended instead of cerium. The different types of promoters employed are encouraged to be further explored.
5. There are various types of carbon deposited on the catalyst. The actual type and its amount formed are essential as this information can be used to undergo further research on the effective methods of coke reduction.
6. FTIR is recommended to determine the species present on the catalyst. It can clearly point out species. Elemental analysis is important in catalysis research.

References

- Cichy, M., & Borowiecki, T. (n.d.). Steam reforming of glycerol on the Ni-Re catalysts, 2(1).
- Czekaj, I., Struis, R., Wambach, J., & Biollaz, S. (2011). Sulphur poisoning of Ni catalysts used in the SNG production from biomass: Computational studies. *Catalysis Today*, 176(1), 429–432. doi:10.1016/j.cattod.2010.10.078
- El Doukkali, M., Iriondo, a., Arias, P. L., Cambra, J. F., Gandarias, I., & Barrio, V. L. (2012). Bioethanol/glycerol mixture steam reforming over Pt and PtNi supported on lanthana or ceria doped alumina catalysts. *International Journal of Hydrogen Energy*, 37(10), 8298–8309. doi:10.1016/j.ijhydene.2012.02.154
- Kale, G. R., & Kulkarni, B. D. (2010). Thermodynamic analysis of dry autothermal reforming of glycerol. *Fuel Processing Technology*, 91(5), 520–530. doi:10.1016/j.fuproc.2009.12.015
- Wang, X., Li, M., Wang, M., Wang, H., Li, S., Wang, S., & Ma, X. (2009). Thermodynamic analysis of glycerol dry reforming for hydrogen and synthesis gas production. *Fuel*, 88(11), 2148–2153. doi:10.1016/j.fuel.2009.01.015
- Wilson, K., Lee, A. F., & Dacquin, J. (2012). *Catalysis for Alternative Energy Generation*. (L. Gucci & A. Erdőhelyi, Eds.). New York, NY: Springer New York. doi:10.1007/978-1-4614-0344-9
- Sánchez, E.A., D'Angelo, M. A., Comelli, R.A. (2010). Hydrogen production from glycerol on Ni/Al₂O₃ catalyst. *Int. J. Hydrogen Energy*, **35**: 5902-5907. doi:10.1016/j.ijhydene.2009.12.115
- Trimm, D.L., Adesina, A.A., Praherso, Cant, N.W. (2004). The conversion of gasoline to hydrogen for on-board vehicle applications. *Catal. Today*, **93–95**: 17-22. doi:10.1016/j.cattod.2004.05.018
- Gallego, G.S. & Batiot-Dupeyrat, C. (2008). Dry reforming of methane over Lani1 yByO₃±[Delta] (B = Mg, Co) Perovskites used as catalyst precursor. *Appl. Catal. A: Gen.*, **334(1-2)**: 251-258. doi:10.1016/j.apcata.2007.10.010
- Gao, J., Hou, Z.Y., Lou, H., Zheng, & X.M. (2011). Chapter 7: Dry (CO₂) Reforming.

- Fuel Cells*, **7**:191-221. doi:10.1016/B978-0-444-53563-4.10007-0
- Liu, L. (2012). Exploring hybrid nickel catalysts on doped-ceria supports for the autothermal reforming of surrogate liquid fuel. *Department Of Chemical & Biomolecular Engineering National University Of Singapore*. pp: 1-197.
- Bartholomew, C.H. (2001). Mechanisms of catalyst deactivation. *App. Catal. A: Gen.*, **212**: 17–60. doi:10.1016/S0926-860X(00)00843-7.
- Dutrow, B.L. & Clark, C.M. (n.d). X-ray Powder Diffraction (XRD). Retrieved from http://serc.carleton.edu/research_education/geochemsheets/techniques/XRD.html
- Brunauer, S., Emmett, P.H. & Teller E. (1938). Adsorption of gases in multimolecular layers. *J Amer Chem Soc*, **60**, 309-319.
- Langmuir, I. (1916). The constitution and fundamental properties of solids and liquids. *J Amer Chem Soc*, **38**, 2221-2267.
- Hossein, M.K. (2012). FE-SEM and EDX characterization of sand blasted and sulphuric acid etched of novel. *Aus. J. of Basic and App. Sci.*, **6(6)**: 125-131. ISSN 1991-8178
- Natesakhawat, S., Watson, R.B., Wang, X.Q., & Ozkan U.S. (2005). Deactivation characteristics of lanthanide-promoted sol–gel Ni/Al₂O₃ catalysts in propane steam reforming. *J. of Catal.*, **234**: 496–508. doi:10.1016/j.jcat.2005.07.014
- Iriondo, Barrio, V.L., Cambra, J.F., Arias, P.L., Guemez, M.B., Sanchez-Sanchezb, M.C., Navarro, R.M., Fierro, J.L.G. (2010). Glycerol steam reforming over Ni catalysts supported on ceria and ceria-promoted alumina. *Int. J. Of Hydrogen Energy*, **35**:11622-11633. doi:10.1016/j.ijhydene.2010.05.105

- ISO 9277, (2010). Determination of The specific surface area of solids by gas adsorption
- BET method. *Int. Standard*. Pp. 1-24.
- Cheng, C.K., Foo, S.Y., & Adesina, A.A. (2011). Steam reforming of glycerol over
Ni/Al₂O₃ catalyst. *Catal. Today*, **178**: 25-33. doi:10.1016/j.cattod.2011.07.011
- Cheng, C.K. (2011). Synthesis gas production from glycerol steam reforming over
alumina supported bimetallic Co-Ni catalyst. *University Of New South Wales
Sydney Australia*, p.p. 1-259
- Bergeret, G. & Gallezot, P. (1997). Particle size and dispersion measurements, in:
Ertl, G., Nozinger, H. & Weitkamp, J. (Eds.). *Handbook of Heterogeneous Catalysis*
Weinheim.
- Kandaswamy, D., Rajan, K.J., Venkateshbabu, N., & Porkodi, I. (2012). Shear bond
strength evaluation of resin composite bonded to glass-ionomer cement using self-
etching bonding agents with different Ph: In Vitro study. *J Conserv Dent.*, **15(1)**:
27–31. doi: 10.4103/0972-0707.92602
- Brabazon, D., & Raffer, A. (2010). Chapter 3 - Advanced characterization techniques for
nanostructures. *Emerging Nanotechnol. for Manufac.*, pp: 59-91. ISBN: 978-0
8155-1583-8
- Lausmaa, J., B. Kasemo *et al.*, (1990). Surface spectroscopic characterization of titanium
implant materials. *App. Surf, Sci.*, **44(2)**: 133-146. Doi:10.1016/0169
4332(90)90100-E
- Sahle-Demessie, E., Zhao, A., Salamon, A.W. (2011). A study of aged carbon nanotubes

- by Thermogravimetric Analysis. *PerkinElmer Inc.*, pp. 1-4. Retrieved from http://www.perkinelmer.com/content/applicationnotes/APP_NanotubestudybyThermogravimetricAnalysis.pdf
- Tzeng, S.S., Wu, T.Y., Chang, T.Y., Yang, C.T., Chou, C.I., Lin, C.J. (2010). Study of oxidation of carbon fibers using resistance measurement. *J. Mater. Eng. Perform.*, **19(9)**: 1352-1356. doi: 10.1007/s11665-010-9628-y
- Dr. Anderson, C.R., (2012). Thermogravimetry (TG) or Thermogravimetric Analysis (TGA) or Thermal Gravimetric Analysis. *Anderson Materials Evaluation, Inc.* Retrieved from <http://www.andersonmaterials.com/tga.html>
- Wang. XD, Li. SR, Wang. H, Liu. B, Ma. XB. Thermodynamic analysis of glycerine steam reforming. *Energy Fuels* 2008;22(6):4285–91.
- Adhikari. S, Fernando. S, Gwaltney. SR, To SDF, Bricka RM, Steele PH, et al. The thermodynamic analysis of hydrogen production by steam reforming of glycerol. *Int J Hyd Energy* 2007;32:2875–80.
- Simonetti DA, Kunkes EL, Dumesic JA. Gas-phase conversion of glycerol to synthesis gas over carbon-supported platinum and platinum–rhenium catalysts. *J Catal* 2007;247(2):298–306.
- Dry, M.E. The Fischer-Tropsch process: 1950–2000. *Catal Today* 2002;71(3–4):227–41.
- Juan-Juan, J., Roman-Martinez, M.C., Illán-Gómez, M.J. (2006). Effect of potassium content in the activity of K-promoted Ni/Al₂O₃ catalysts for the dry reforming of methane. *Appl Catal A: Gen.* 301:9-15. doi:10.1016/j.apcata.2005.11.006

- Luna, A.E.C., Iriarte, M.E. (2008). Carbon dioxide reforming of methane over a metal modified Ni-Al₂O₃ catalyst. *Appl Catal A: Gen.*, 343:10-15.
doi:10.1016/j.apcata.2007.11.041
- Roh, H.S., Jun, K.W., (2008). Carbon dioxide reforming of methane over ni catalysts supported on Al₂O₃ modified with La₂O₃, MgO, and CaO. *Catal Surv Asia*. 12:239-252. doi 10.1007/s10563-008-9058-0
- Nielsen, R. & Hansen, J.H.B. (1993). CO₂-reforming of methane over transitionmetals. *J.Catal.* 44(1):38-49. doi: 10.1006/jcat.1993.1312
- Hou, Z.Y., & Yashima, T. (2003). Small amounts of Rh-Promoted Ni catalysts for methane reforming with CO₂. *Catal. Lett.* 89:193-197. Retrieved from <http://link.springer.com/content/pdf/10.1023%2FA%3A1025746211314>
- Lee, W.Y., Hanna, J., & Ghoniem, A.F. (2012). Improvements to predictions of carbon deposition on the nickel anode of a SOFC under open-circuit conditions. Massachusetts Institute of Technology, Cambridge. Pp. 1-43. Retrieved from <http://hyksos.mit.edu/rgdWebFiles/HannaJES2012.pdf>
- Lemonidou, A.A., Goula, M.A., Vasalos, I.A. (1998). Carbon dioxide reforming of methane over 5 wt.% nickel calcium aluminate catalysts ± effect of preparation method. *Catal. Today*, 46: 175-183. P II: S0920-5861(98)00339-3.
- Seth, D. (2002). Hydrogen futures: Toward a sustainable energy system. *Int. J. of Hydrogen Energy*, 27:235-264. PII:S0360-3199(01)00131-8
- Dave, R. (2010). Greenhouse gases: methane. *The Encyclopedia of Earth*. Retrieved from <http://www.eoearth.org/article/Methane?topic=49554>
- Saunders, G.J., & Kendall, K. (2002). Reactions of hydrocarbons in small tubular

- SOFCs. *J. of Power Sources*, 106:258–263. PII: S0378-7753(01)01067-9.
- Kelemen, S.R. (2007). Tracking the origins of fossil fuels. U.S. Department of Energy, Office of Science. Retrieved from <http://www.aps.anl.gov/Science/Highlights/2007/20070529.htm>
- Jiang, Z.X., Lü, H.Y., Zhang, Y.N., & Li, C. (2011). Oxidative desulfurization of fuel oils. *Chi. J. Of Catal.*, 32: 707–715. doi: 10.1016/S1872-2067(10)60246-X
- Salbilla, D.L., Kolmetz, K., Cheah P.S., & Soyza, C.A. (2002). Fluidized catalytic cracker catalyst selection: equilibrium catalyst quality and considerations for selections. Retrieved from [http://kolmetz.com/pdf/articles/FCC CatalyticCracking-Rev-intro.pdf](http://kolmetz.com/pdf/articles/FCC_CatalyticCracking-Rev-intro.pdf)
- A. Djaidja, S. Libs, A. Kiennemannb, A. Barama, (2006). Characterization and activity in dry reforming of methane on NiMg/Al and Ni/MgO catalysts, *Catalysis Today* 113, 194-200
- Adriana Campos, Josue M. Filho, Alcinea C. Oliveira. (2012). Mesoporous catalysts for dry reforming of methane: Correlation between structure and deactivation behavior of Ni-containing catalysts, *international journal of hydrogen energy* 37,12281-12291
- Daza, C. E., Gallego, J., Mondragón, F., Moreno, S., & Molina, R. (2010). High stability of Ce-promoted Ni/Mg–Al catalysts derived from hydrotalcites in dry reforming of methane. *Fuel*, 89, 592–603.
- Y. Hu, E. Ruckenstein, High resolution transmission electron microscopy study of carbon deposited on the NiO /MgO solid solution catalysts, *Journal of Catalysis*, 184 (1999) 298-302.
- Lucredio, A.F., Jerkiewickz, G., & Assaf, E.M. (2007). Nickel catalysts promoted with cerium and lanthanum to reduce carbon formation in partial oxidation of methane reactions. *Appl. Catal., A.* 333:90-95. doi:10.1016/j.apcata.2007.09.009

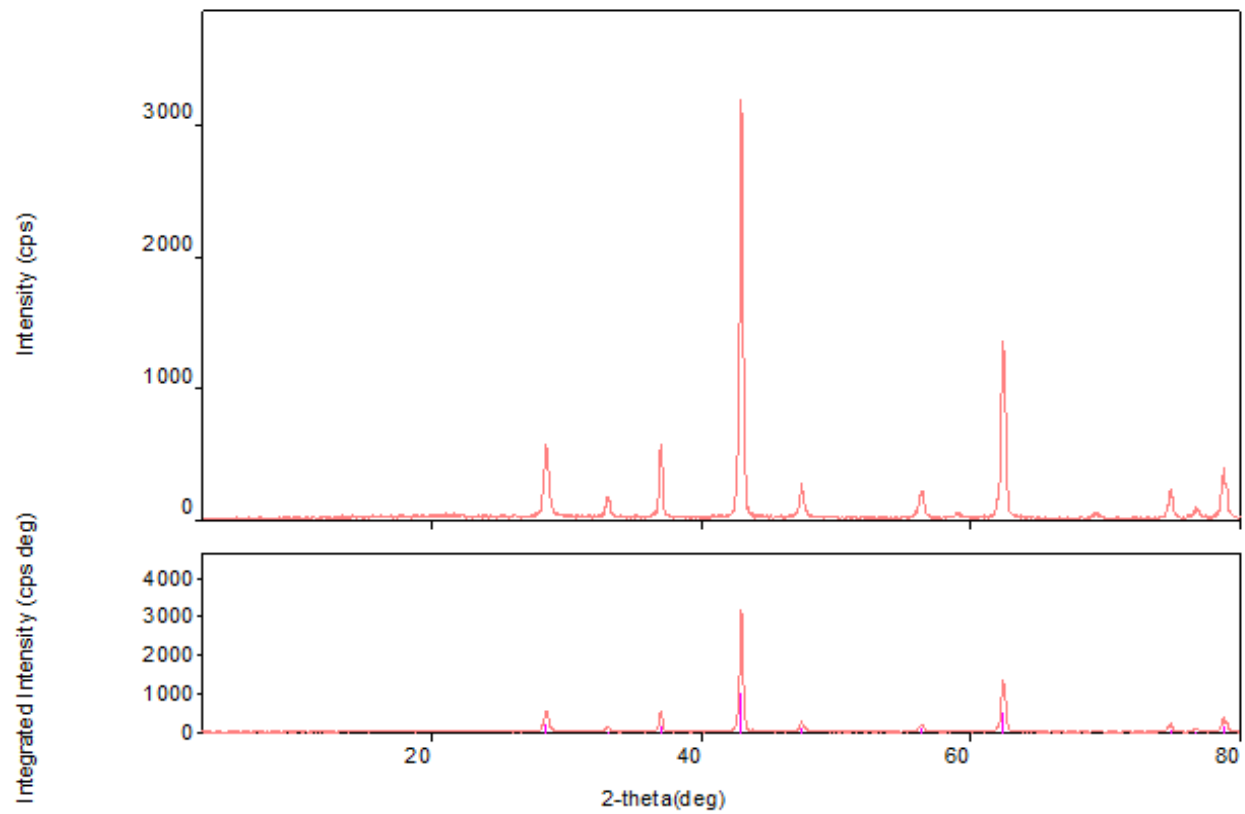
- Nilsson, M., Jansson, K., Jozsa, P., & Pettersson, L.J. (2009). Catalytic properties of Pd supported on ZnO/ZnAl₂O₄/Al₂O₃ mixtures in dimethyl ether autothermal reforming. *Appl. Catal., B.* 86:18-26. doi:10.1016/j.apcatb.2008.07.012
- Yoon, S., Kang, I., & Bae, J., (2009). Suppression of ethylene-induced carbon deposition in diesel autothermal reforming. *Int. J. Hydrogen Energy.* 34:1844-1851. doi:10.1016/j.ijhydene.2008.12.016
- Lim, S.S., Lee, H.J., Moon, D.J., Kim, J.H., Park, N.C., Shin, J.S., & Kim, Y.C. (2009). Autothermal reforming of propane over Ce modified Ni/LaAl₂O₃ Perovskite-type catalysts. *Chem. Eng. J. (Lausanne)*, 152:220-226. Retrieved from <http://z150.com/120081019158339015.html>
- Escritori, J.C., Dantas, S.C., Soares, R.R., & Hori, C.E. (2009). Methane autothermal reforming on Nickel-Ceria-Zirconia based catalysts. *Catal Commun.*, 10:1090-1094. doi:10.1016/j.catcom.2009.01.001
- Cheng C.K., (2011). Synthesis gas production from glycerol steam reforming over alumina supported bimetallic Co-Ni catalyst. The University of New South Wales. Pp. 1-259.
- Wang, A.W. (1997). Poison resistant catalyst development and testing: design and construction of the alternative fuels field test unit and liquid phase methanol feedstock and catalyst life testing at Eastman Chemical Company Kingsport, TN. United States Department of Energy. Pp. 1-64. Retrieved from http://www.netl.doe.gov/technologies/coalpower/fuelcells/publications/fuelcell/fc_cleanup/Topical%20Report%20-%20AFFTU%20at%20Kingsport.pdf
- Babich, I.V., & Moulijn, J.A. (2002). Science and technology of novel processes for deep desulfurization of oil refinery streams: A review. *Fuel.* 82: 607–631. PII: S00162361(02)00324-1

- Lakshapatri, S.L. & Abraham, M.A. (2009). Deactivation due to sulfur poisoning and carbon deposition on Rh-Ni/Al₂O₃ catalyst during steam reforming of sulfur-doped N-hexadecane. *Appl. Catal., A*, 364:113-121. doi:10.1016/j.apcata.2009.05.035
- Czekaj, I., Struis, R., Wambach, J., & Biollaz, S. (2011). Sulphur poisoning of Ni catalysts used in the SNG production from biomass: Computational studies. *Catalysis Today*, 176(1), 429–432. doi:10.1016/j.cattod.2010.10.078
- Sehested, J. (2004). Sintering of nickel steam-reforming catalysts: effects of temperature and steam and hydrogen pressures. *Journal of Catalysis*, 223(2), 432–443. doi:10.1016/j.jcat.2004.01.026
- C.H. Bartholomew, *Appl. Catal. A* 107 (1993) 1.
- J.T. Richardson, J.G. Crump, *J. Catal.* 57 (1979) 417.
- Smejkal, Q; Linke, D; Bentrup, U, M. Baerns, et al. *APPLIED CATALYSIS A-GENERAL* Volume: 268 8 (2004), Issue: 1-2, p.: 67.

APPENDICES

Appendices A

5 wt% Ce-Ni/MgO catalyst

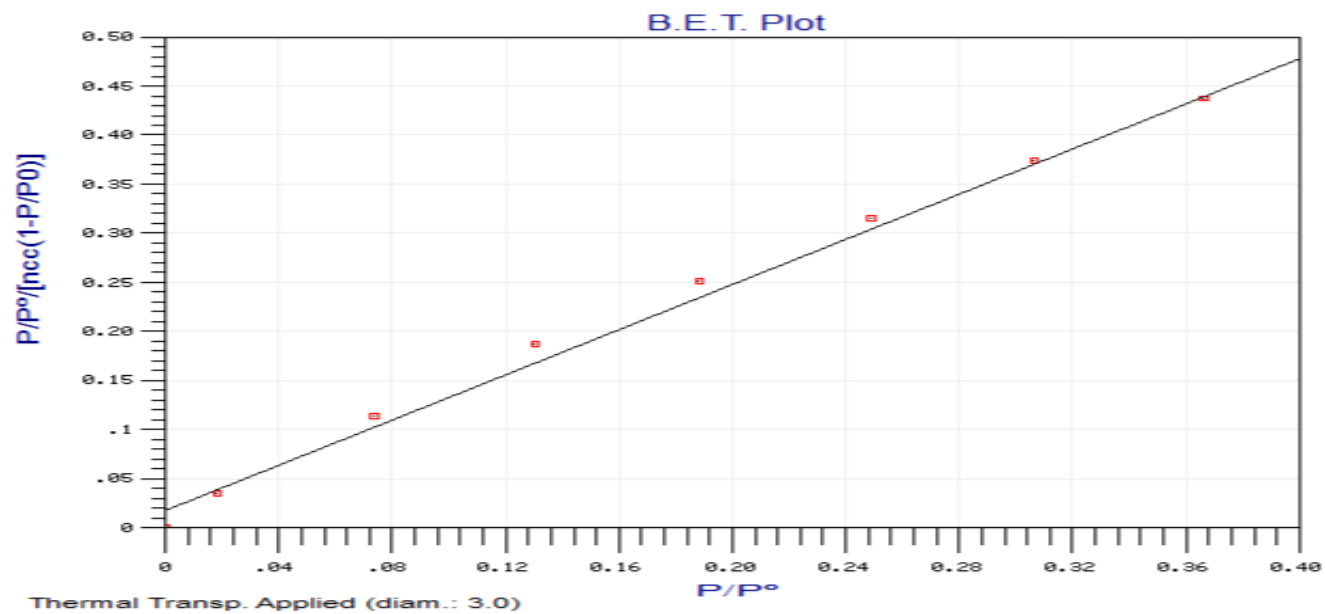


Peak list

2-theta (deg)	d (ang.)	Height (cps)	Int. I(cps*deg)	FWHM(deg)	Size	Phase name
28.531(10)	3.1259(10)	359(19)	172(2)	0.353(8)	242(5)	Unknown,
33.053(19)	2.7079(15)	93(10)	40.9(14)	0.367(15)	236(10)	Unknown,
36.997(9)	2.4277(6)	415(20)	113.8(16)	0.204(8)	429(17)	Unknown,
42.987(5)	2.1023(2)	2443(49)	693(5)	0.214(4)	417(8)	Unknown,
47.457(16)	1.9142(6)	183(14)	93.2(15)	0.373(12)	243(8)	Unknown,
56.36(2)	1.6311(6)	147(12)	75.3(15)	0.37(2)	256(15)	Unknown,
59.06(7)	1.5627(16)	21(5)	11.3(12)	0.51(5)	186(18)	Unknown,
62.407(5)	1.48681(11)	1126(34)	370(3)	0.244(6)	398(9)	Unknown,
74.836(14)	1.2677(2)	163(13)	64.0(14)	0.315(15)	331(16)	Unknown,
76.76(4)	1.2407(6)	42(6)	19.7(13)	0.44(3)	241(19)	Unknown,
78.786(7)	1.21373(9)	300(17)	117.5(19)	0.290(9)	370(11)	Unknown,

Appendices B

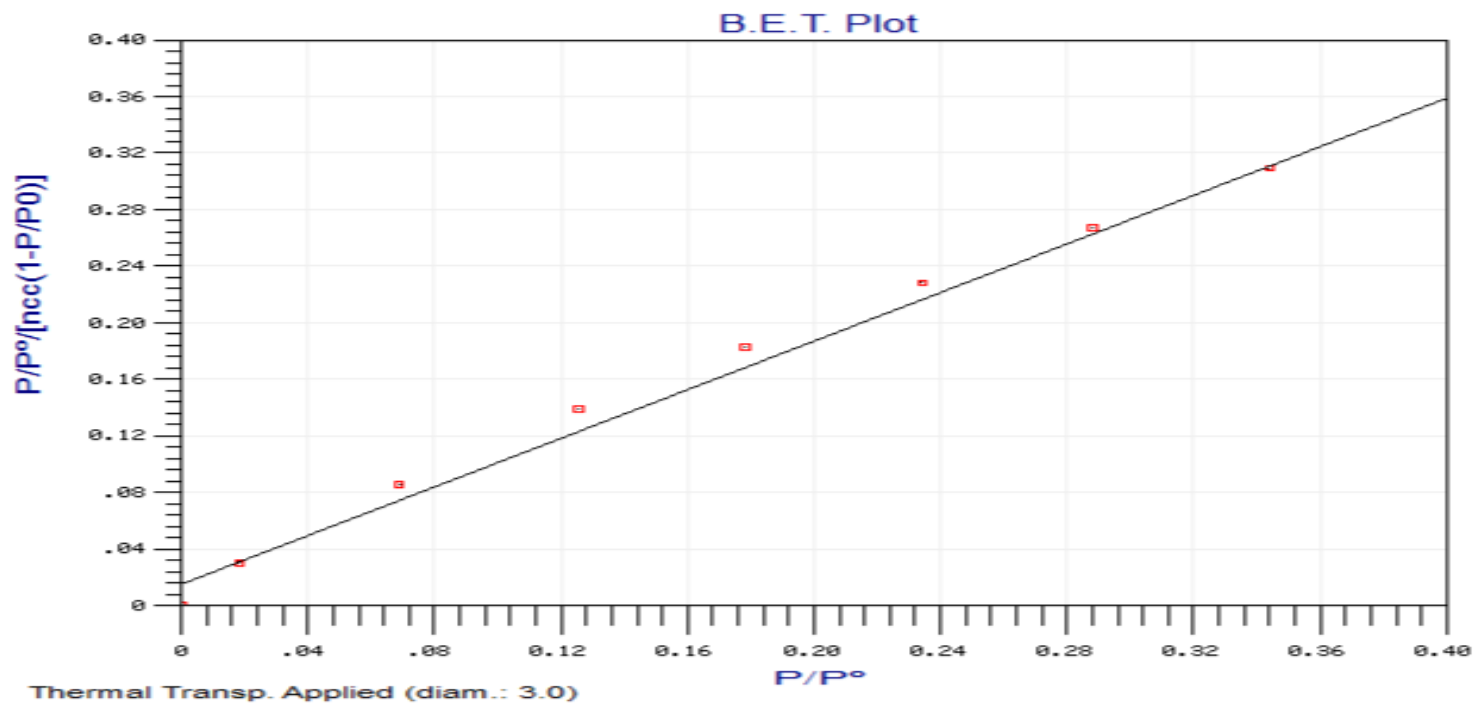
i) 3 wt % Ce-Ni/MgO catalyst



Surface Area calculation results

Calculation Method: B.E.T.
Initial-Final P/P^0 : 0 - .4
Monolayer Volume (ncc/g): .8541248
Specific Surface Area (m^2/g): 10.59064
C Value of BET Equation: 69.97855
Correlation Factor: .9970396

ii) 5 wt% Ce-Ni/MgO catalyst

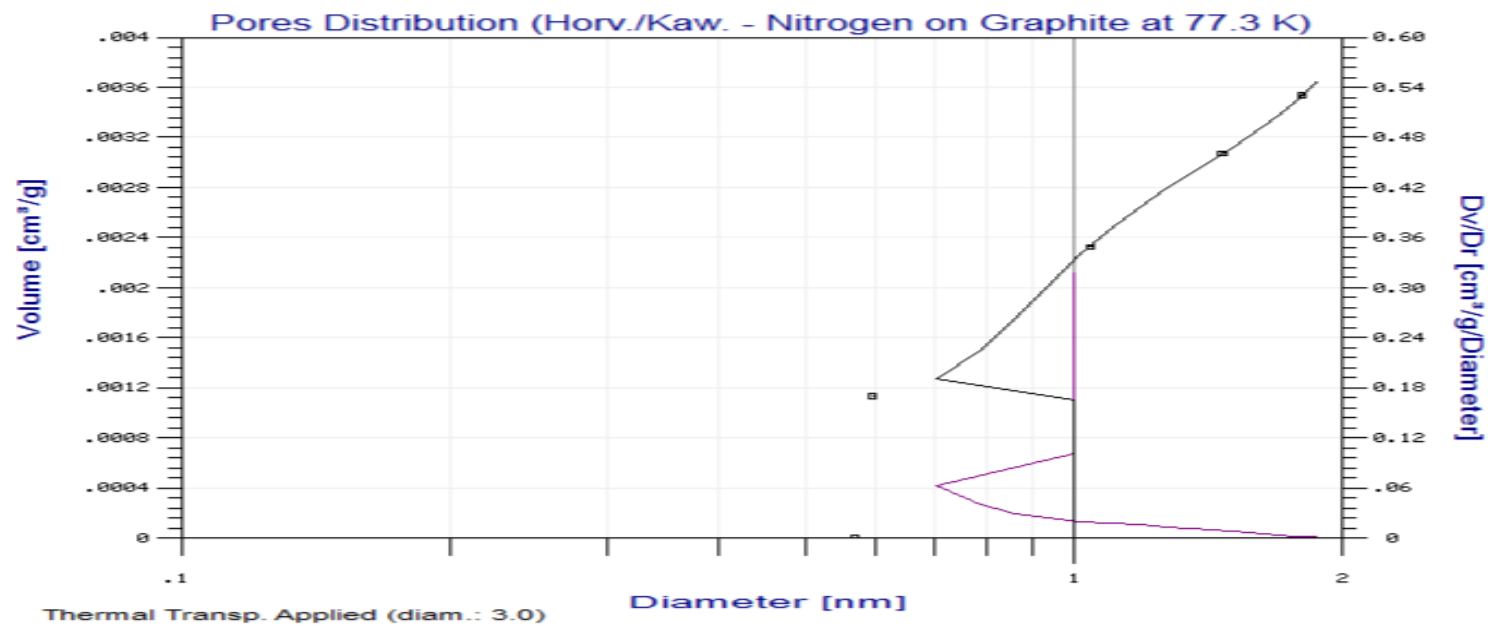


Surface Area calculation results

Calculation Method: B.E.T.
Initial-Final P/P°: 0 - .4
Monolayer Volume (ncc/g): 1.142086
Specific Surface Area (m²/g): 13.99765
C Value of BET Equation: 58.2858
Correlation Factor: .995577

Appendices C

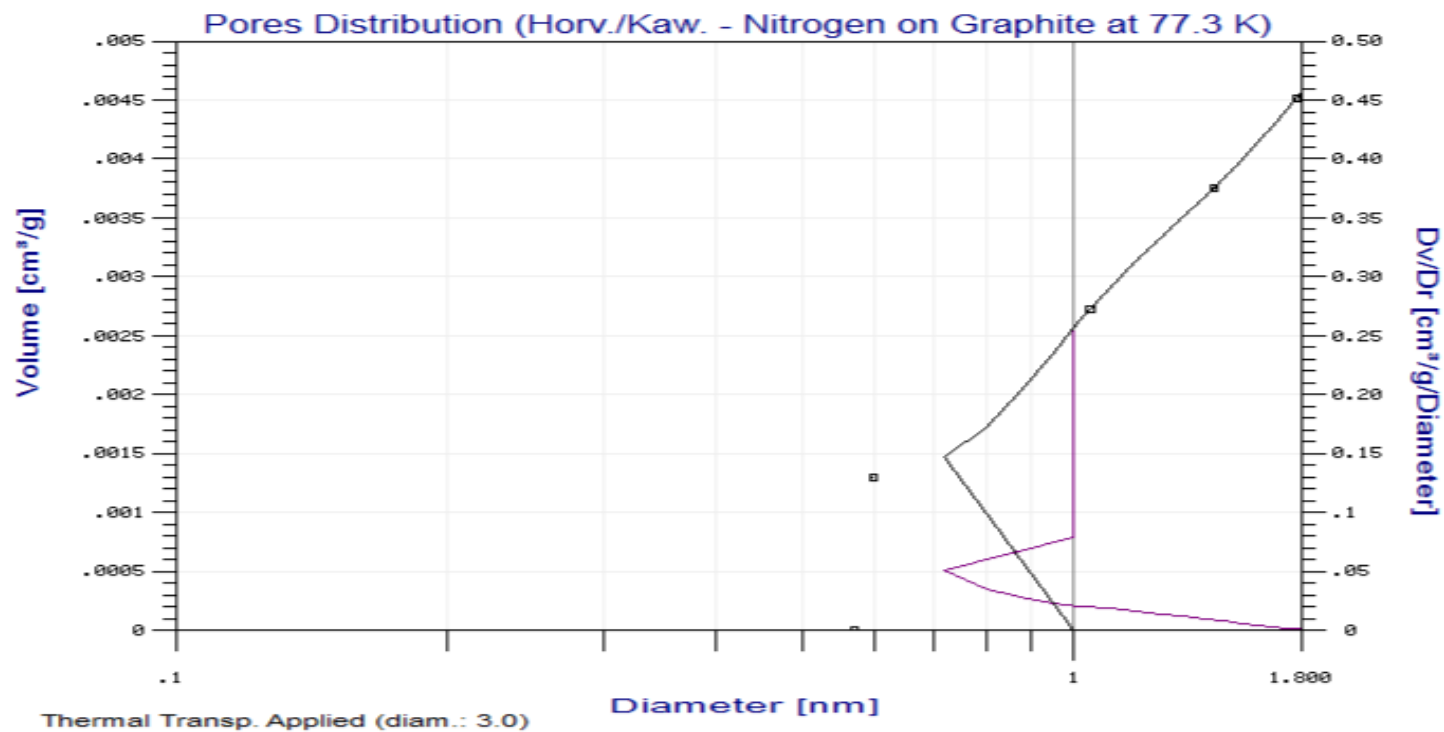
i) 3 wt% Ce-Ni/MgO catalyst



Pore size results

Calculation method: Horvat & Kavazoe
Model: Nitrogen on Graphite at 77.3 K
Pore Size Range (Diameter): 0.0 - 0.15
Cumulative Volume (cm³/g): 0.0035
Maximum Diameter (nm): .5953743
Average Diameter (nm): .8847383

ii) 5 wt % Ce-Ni/MgO catalyst



Pore size results

Calculation method: Horvat & Kavazoe
Model: Nitrogen on Graphite at 77.3 K
Pore Size Range (Diameter): 0.0 - 0.15
Cumulative Volume (cm³/g): 0.0045
Maximum Diameter (nm): .5987141
Average Diameter (nm): .96458

Appendices D

